P–T–X Relationships Deduced from Corona Textures in Sapphirine–Spinel–Quartz Assemblages from Paderu, Southern India

by R. K. LAL[1], D. ACKERMAND[2] AND H. UPADHYAY[1]

[1] *Department of Geology, Banaras Hindu University, Varanasi 221005, India*
[2] *Mineralogisches Institut der Universitaet Kiel, Olshausenstrasse 40, 2300 Kiel, Federal Republic of Germany*

(*Received 8 July 1985; revised typescript accepted 3 June 1987*)

ABSTRACT

The sapphirine (Sa)–spinel (Sp)–quartz (Qz)-bearing rocks from Paderu occur as lenticular enclaves within the Precambrian khondalite–charnockite terrane of southern India. In addition these rocks contain orthopyroxene (Opx), sillimanite (Sill), garnet (Gt), cordierite (Cd), biotite, potash feldspar (Kf), plagioclase, and symplectites of Cd–Kf–Qz–Opx. The symplectites may have formed from the breakdown of osumilite. Grain contacts of sapphirine and spinel with quartz are rarely observed and the incompatibility with quartz during later stages is displayed by the development of several types of polymineralic reaction coronas. The coronas in the different rock types A, B, etc. are (minerals listed from core to rim of corona):
(*A-1*) *sapphirine-bearing rock type without spinel:* Sa–Sill–Opx, Sa–Sill–Cd, Sa–Cd–Opx;
(*A-2*) *sapphirine and spinel-bearing:* Sp–Sa–Sill–Opx–Qz, Sp–Sa–Sill, Sp–Sa–Opx, Sp–Sill–Opx, Sp–Sa–Sill–Gt–Qz, Sa–Sill–Opx, Sp–Sa–Sill–Opx, Sa–Sill–Opx–Gt, Sp–Sa–Opx–Gt, Sp–Sa–Sill–Gt; and (*B*) *spinel-bearing but sapphirine free*: Sp–Sill–Opx, Sp–Sill–Gt, Sp–Cd. Commonly the coronas in the rock type A 2 and B also contain ilmeno-hematite ± corundum in the core in association with spinel. These rock types also provide textural evidence for later crystallization of Cd, Cd + Sa, and Gt + Qz from Opx + Sill ± Qz and Gt + Sill + Qz.

Sapphirine is aluminous (near $7(Mg, Fe^{2+})O \cdot 9(Al, Fe^{3+})_2O_3 \cdot 3SiO_2$) and contains up to 12·2 wt. per cent iron as FeO. Orthopyroxene is also aluminous, containing up to 10·4 wt. per cent Al_2O_3. Sapphirine and spinel have relatively high contents of Fe_2O_3. X_{Mg} in the Fe–Mg minerals increases from rock type B to A2 to A1.

A sequence of reactions has been deduced from coronas and other reaction textures, and from the phase compatibility relations in the FeO–MgO–Al_2O_3–SiO_2–H_2O system. The *P–T–X* relationships from geothermobarometry and petrogenetic grids, viz. $\mu_{Fe_2O_3}$ vs. μ_{FeO} and μ_{H_2O} vs. $\mu_{Fe_2O_3}$, suggest: (1) a retrograde, mildly decompressive trajectory from 900 ± 60 °C/$6{\cdot}5 \pm 0{\cdot}7$ kb (core) to 760 ± 50 °C/5 $\pm 0{\cdot}6$ kb (rim); and (2) the observed mineralogy of the coronas and reactions deduced from them are dependent on the relative FeO, Fe_2O_3, and H_2O contents of the rocks (μ_{FeO}, $\mu_{Fe_2O_3}$, and μ_{H_2O}).

INTRODUCTION

Sapphirine–quartz associations have attracted the attention of petrographers and experimental petrologists, because they indicate medium to high-pressure and high-temperature metamorphic conditions. The experimental studies in the MgO–Al_2O_3–SiO_2–H_2O system (MASH) (Schreyer & Seifert, 1969; Hensen & Green, 1971; Chatterjee & Schreyer, 1972), the anhydrous MgO–Al_2O_3–SiO_2 (MAS) system (Newton, 1972) and the FeO–MgO–Al_2O_3–SiO_2–H_2O (FMASH) system (Hensen & Green, 1971) give information about the metamorphic conditions and the reactions involved in the formation of sapphirine–quartz associations. Many of the reactions studied experimentally have been

documented by reaction coronas observed in sapphirine–quartz-bearing rocks (Caporuscio & Morse, 1978; Ellis *et al.*, 1980; Droop and Bucher-Nurminen, 1984).

Although the MAS and FMAS model systems are good approximations of many sapphirine–quartz-bearing rocks (Ellis *et al.*, 1980; Grew 1980*a*), other rocks with such assemblages deviate from these model systems due to the presence of Fe_2O_3, or less commonly of Cr_2O_3 (Caporuscio & Morse, 1978). Therefore, it is desirable to investigate these assemblages in terms of more complex chemical systems in order to determine the effects of deviations from the model systems. This in turn will help us to better interpret the metamorphic conditions inferred from these assemblages.

Sapphirine–quartz associations have been reported from eight areas worldwide: Enderby Land, Antarctica (Dallwitz, 1968; Ellis *et al.*, 1980; Grew, 1980*a*); Peekskill, New York (Caporuscio & Morse, 1978); Wilson Lake, Labrador (Morse and Talley, 1971; Meng & Moore, 1972; Bourne, 1978); Labwor, Uganda (Nixon *et al.*, 1973); the Chogar Complex, Eastern Siberia (Karsakov *et al.*, 1975); Gruf Complex, Central Alps (Droop & Bucher-Nurminen, 1984) and Limpopo Belt (Schreyer *et al.*, 1984). Except for Peekskill, where sapphirine–quartz assemblages are from contact metamorphosed xenoliths in peridotite, all the other localities are regionally metamorphosed granulite facies terranes.

In southern India several occurrences of sapphirine-bearing rocks are known, but the association sapphirine + spinel + quartz is reported only from Paderu, Eastern Ghats (Rao, 1980; Grew, 1982). During this study we found several samples containing sapphirine–quartz and spinel–quartz associations in textural equilibrium, as well as a number of samples where reaction coronas had developed between these mineral pairs. From these, a sequence of retrograde reactions can be inferred.

In our paper we will consider: (1) the different types of corona textures in sapphirine-bearing rocks of the area, including several types so far not reported from any other terrane, with reference to the reactions involved in their formation; (2) a chemographic study in the FMASH system; (3) the P–T–X relationships in these rocks during metamorphic crystallization based on geothermobarometry and petrogenetic grids, viz. P vs. T, $\mu_{Fe_2O_3}$ vs. μ_{FeO} and μ_{H_2O} vs. $\mu_{Fe_2O_3}$; and (4) a comparison of the P–T–X regime with other localities of sapphirine–spinel–quartz rocks.

GEOLOGICAL SETTING

The Paderu area, which is in the Visakhapatnam district of Andhra Pradesh, constitutes part of the Precambrian khondalite–charnockite terrane of the Eastern Ghats (Fig. 1). In addition to khondalites and charnockites, other rock types in the Eastern Ghats are two pyroxene granulites (± garnet), leptynites, garnetiferous leptynites, garnet–biotite-gneisses, calc-granulities, sapphirine–spinel-bearing granulites, etc. These are intruded by granites, norites, anorthosite suite rocks, etc. The khondalite–charnockite and associated rocks have been multiply deformed and were subjected to a major episode of granulite-facies metamorphism followed by retrogression. Three phases of deformation have been recognized in the Eastern Ghats: (a) a D_1 deformation, during which strongly appressed isoclinal folds (F_1) formed with axial trends in the east-northeast–west-southwest and northeast–southwest directions; (b) open cross-folds (F_2) trending north–south and north-northwest–south-southeast generated during the D_2 deformation; and (c) cross folding (F_3) of the earlier folds along approximately east–west trending axes into gentler antiforms and synforms during the D_3 formation (Narayanaswamy, 1964; Sriramdas & Rao, 1979; Sarkar *et al.*, 1981). Sarkar *et al.* (1981) suggested that the D_1 and D_2 deformations and associated high-grade metamorphism occurred during the 3000 ± 100 Ma and 2600 ± 100 Ma tectonother-

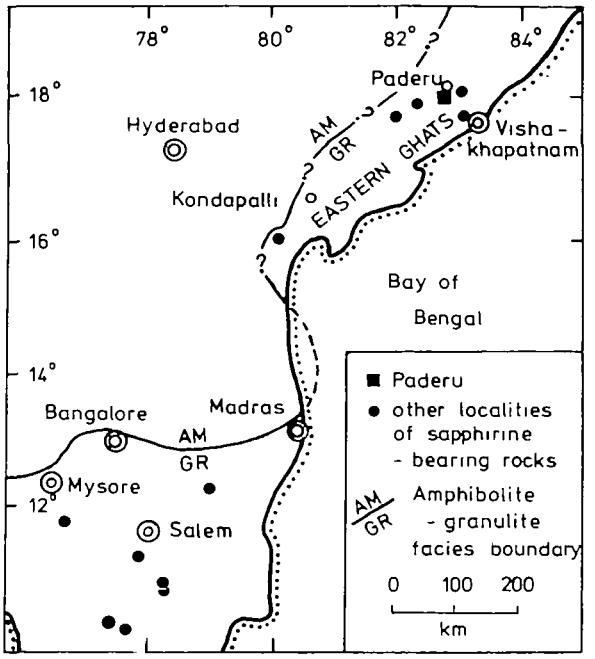

FIG. 1. Map showing the location of the Paderu area. Other localities of sapphirine-bearing rocks from Eastern Ghats, India are also shown (based on Grew, 1982). Am—amphibolite facies, Gr—granulite facies. The amphibolite–granulite facies transition is based on Raith *et al.* (1983) and our unpublished data.

mal events respectively, whereas the D_3 deformation and syntectonic emplacement of the anorthositic suite took place during 1400 ± 100 Ma (see below).

Radiometric age data of the rocks of the Eastern Ghats are too few to reconstruct the sequence of tectonothermal events. A possible sequence may be proposed, based on available data on isotopic studies of these rocks:

(1) a khondalite from Puri, Orissa yielded a Rb–Sr whole rock age of 3090 Ma, which is the oldest recognizable event (Perraju *et al.*, 1979). This corresponds to a whole rock Rb–Sr age of 3070 Ma for the garnet–sillimanite gneiss from Kerala (Crawford, 1969) and to the 3000 Ma event of high-grade, amphibolite-facies metamorphism and migmatization in the Peninsular Gneiss Complex of Karnataka and Tamil Nadu in southern India (cf. Ramakrishnan *et al.*, 1984).

(2) Rb–Sr whole-rock age of 2482 and 2695 Ma for the khondalite and intermediate charnockite, respectively, from Visakhapatnam (Perraju *et al.*, 1979) and a U–Pb zircon age of 2600 Ma of khondalite from Puri (Vinogradov *et al.*, 1964) correspond to the 2600–2500 Ma event, during which prograde greenschist- to granulite-facies metamorphism took place in Karnataka and Tamil Nadu (Crawford, 1969; Buhl *et al.*, 1983; Raith *et al.*, 1983). Besides these, significantly younger ages have also been reported for these rocks e.g., 1570 ± 70 Ma for detrital monazite from Cuttack, Orissa (Holmes, 1955); Rb–Sr whole-rock ages of 2129–1381 Ma for khondalites, charnockites, garnet–sillimanite-gneisses and leptynites from Visakhapatnam (Aswathanarayan, 1964; Crawford, 1969; Perraju *et al.*, 1979); Rb–Sr whole-rock ages of 1211 Ma for leptynites from Puri, 1369–1000 Ma for garnetiferous gneisses and porphyritic quartzo-feldspathic rock from Srikakulam, Andhra Pradesh (Perraju *et al.*, 1979); 1388 ± 22 Ma for xenoliths of khondalite and mafic granulite in

the anorthositic igneous suite from Chilka Lake, Orissa (Sarkar *et al.*, 1981). These ages of the granulite-facies rocks may represent resetting of the radiometric clock during the later thermal events, due to several phases of igneous activity in these areas.

(3) Radiometric age data for later igneous intrusive activity are: Rb–Sr whole-rock ages 2400, 2100 and 1699 Ma for granitic intrusives from Visakhapatnam (Crawford, 1969); a Rb–Sr whole-rock age of 1400 ± 89 Ma from the anorthositic suite and a K–Ar age of 848 ± 16 Ma for plagioclase from a norite dyke in the anorthositic suite of the Chilka lake igneous complex (Sarkar *et al.*, 1981).

(4) K–Ar biotite ages from Visakhapatnam (Aswathanarayan, 1964) and Kondapalli (Grasty & Leelanandam, 1965) indicate the last thermal event (Indian Ocean Cycle) in the Eastern Ghats around 600–450 Ma ago.

The sapphirine–spinel–quartz-bearing rocks in the Paderu (18° 04′N: 82° 42′E) occur as enclaves a few tens of meters long within khondalite or at the contact between khondalite and mafic granulites. These were sampled from the area around Gunduru, about 1·5 km south-southwest of Paderu. The associated rocks of the area include charnockite ($\pm$garnet), enderbites ($\pm$ garnet), mafic two-pyroxene granulites ($\pm$ hornblende, biotite), leptynites, and gneisses with or without garnet.

The sapphirine-bearing rocks of the area have been investigated by Middlemiss (1904), Walker & Collins (1907), Crookshank (1930), Rao (1980), Grew (1982), and Ackermand & Lal (1985). Higgins *et al.* (1979) and Grew (1982, 1983) also reported the occurrence of kornerupine and grandidierite in the silica undersaturated, sapphirine-bearing rocks of the area. A detailed geological map of the area around Paderu is given by Rao (1980). One of us (D. Ackermand), in collaboration with L. H. Rao and K. S. Rao of Andhra University, Waltair, India, is investigating the silica saturated and undersaturated sapphirine-bearing rocks of several other localities near Paderu. The result of this work will be published elsewhere.

TEXTURAL RELATIONS AND METAMORPHIC REACTIONS

The rocks of the area are classified into three main types: (A) sapphirine-bearing; (B) spinel-bearing but sapphirine-free; (C) sapphirine and spinel-free;

Reaction textures observed in these rocks have been arbitrarily subdivided into Early, Middle, and Late Stages based on the textural relations (see below).

Mineral abbreviations are: Opx = orthopyroxene, Sill = sillimanite, Gt = garnet, Sp = spinel, Sa = sapphirine, Qz = quartz, Kf = potash feldspar (hair perthite), Bio = biotite/phlogopite, Cd = cordierite, Plag = plagioclase, An( ) = anorthite (per cent), Ilmeno-hem = ilmeno-hematite, Cn = corundum, Ru = rutile.

The minerals present in the different rock types (Table 1) and their textural relations are summarized below. Not all the minerals listed for each rock type are in textural equilibrium and several mineral assemblages are present in a given section (see below).

Type A: sapphirine-bearing

Without spinel (A-1)

A-1-1: Opx, Sill, Kf, Qz, Cd, Sa, (Cd–Kf–Qz–Opx) symplectite and Bio

A-1-2: Opx, Sill, Gt, Kf, Qz, Cd, Sa, (Cd–Kf–Qz–Opx) symplectite and Bio

With spinel (A-2)

A-2-1: Opx, Sill, Kf, Qz, Sa, Sp, (Cd–Kf–Qz–Opx) symplectite, Bio and Plag (An_{25})

TABLE 1

Modal volume percentage of minerals in different rock types

Rock type	*A-1-1*	*A-2-1*	*A-2-2*	*A-2-2*	*A-2-3*	*A-2-3*	*B-1-2*	*B-2-2*	*C-1*	*C-1*
Sample no.	*17 II*	*303*	*302*	*321*	*320*	*244*	*258*	*252*	*259*	*295*
Garnet	—	—	25	15	8	20	—	5	8	—
Sillimanite	13	10	10	5	7	5	16	10	10	9
Orthopyroxene	25	20	7	16	38	7	15	14	16	12
Spinel	—	+	5	5	+	9	6	4	—	—
Sapphirine	7	+	3	5	+	7	—	—	—	—
Cordierite	20	—	—	—	9	6	15	16	18	—
Quartz	6	20	10	20	+	10	5	5	20	26
Plagioclase	—	6	—	—	—	—	—	6	—	+
(An per cent)		(24·5)						(29·8)		(71·5)
K-feldspar	4	18	6	+	+	+	+	+	+	25
(Cd–Kf–Qz–Opx) symplectite	6	12	20	26	11	23	5	15	24	8
Biotite/ Phlogopite	14	14	9	4	17	5	34	21	4	20
Ilmenite/ Ilmeno-hematite	+	+	+	4	+	+	4	4	+	+
Corundum	—	—	+	+	—	4	—	—	—	—
Rutile	5	—	5	+	+	4	—	—	+	+
Zircon	—	+	—	+	+	+	+	+	+	+

Types of coronas: 17II Sa–Sill–Opx, Sa–Cd–Opx, Sa–Sill–Cd, Sa + Cd symplectite: 303 Sp–Sa–Opx, Sp–Sill–Opx; 302 Sp–Sa–Sill, Sp–Sill–Opx, Sp–Sa–Sill–Gt, Sp–Sill–Opx–Gt, Sp–Sa–Opx, (Sp–Cn–Ilmeno-hem)–Sill–Opx; 321 Sa–Qz, Sp–Qz, Sp–Sill–Opx, Sp–Sa–Sill–Opx–Qz, Sp–Sa–Sill, Sp–Sa–Qz, Sp–Sa–Opx, (Sp–Cn–Ilmeno-hem)–Sill–Opx, 320, Sp–Sa–Opx; 244 Sp–Sill–Opx, Sp–Sa–Opx, Sp–Sa–Sill–Gt, Sp–Sa–Sill–Opx–Gt, Sa–Sill–Opx, Sp–Sa–Sill–Opx; 258 Sp–Sill–Opx, Sp–Cd; 252 Sp–Sill–Opx, Sp–Cd; 259 no corona; and 295 no corona.
—: not observed +: less than 1 modal vol.

A-2-2: Opx, Sill, Gt, Kf, Qz, Sp, Sa, (Cd–Kf–Qz–Opx) symplectite and Bio

A-2-3: Opx, Sill, Gt, Kf, Qz, Cd, Sp, Sa, (Cd–Kf–Qz–Opx) symplectite, Bio and Plag (An_{30})

These rocks also contain minor amounts of zircon, rutile, apatite, and lamellar intergrowths of ilmenite–hematite. In places, coarse prisms of corundum are associated with spinel and ilmeno-hematite/hemo-ilmenite. Corundum is not in textural equilibrium with quartz.

Both the type A and B rocks are dark-coloured, medium- to coarse-grained and migmatitic. A prominent foliation is defined by the alignment of coarse prisms of sillimanite, oval masses containing symplectitic intergrowths of Cd–Kf–Qz–Opx, and rare elongated prisms of orthopyroxene. Coarse-grained orthopyroxene (up to 2 cm long) and garnet (up to 1·6 cm in diameter) contain linear trials of corroded prograde biotite and inequant quartz defining an internal schistosity (S_i) which passes uninterrupted into the external schistosity (S_e).

Sapphirine, which commonly contains spinel inclusions in its core, occurs as small prisms up to 0·1 mm long. It is pleochroic, with X = pale yellow-brown, Y = greenish-blue and Z = deep sapphire-blue. In five samples of type A rocks, sapphirine and spinel are in local grain contact with quartz (Figs. 2A, 2B and 4A), though they are most commonly separated from quartz by the reaction coronas. Osumilite was not found in these rocks (Grew, 1982), but the ubiquitous presence of symplectitic intergrowths of Cd–Kf–Qz–Opx (Fig. 3F) suggests that it may have been stable during the thermal peak of metamorphism. The breakdown of osumilite to this type of symplectite was first suggested by Schreyer & Seifert (1967) and has since been reported by Berg & Wheeler (1976), Ellis *et al.* (1980), and Grew (1982). The

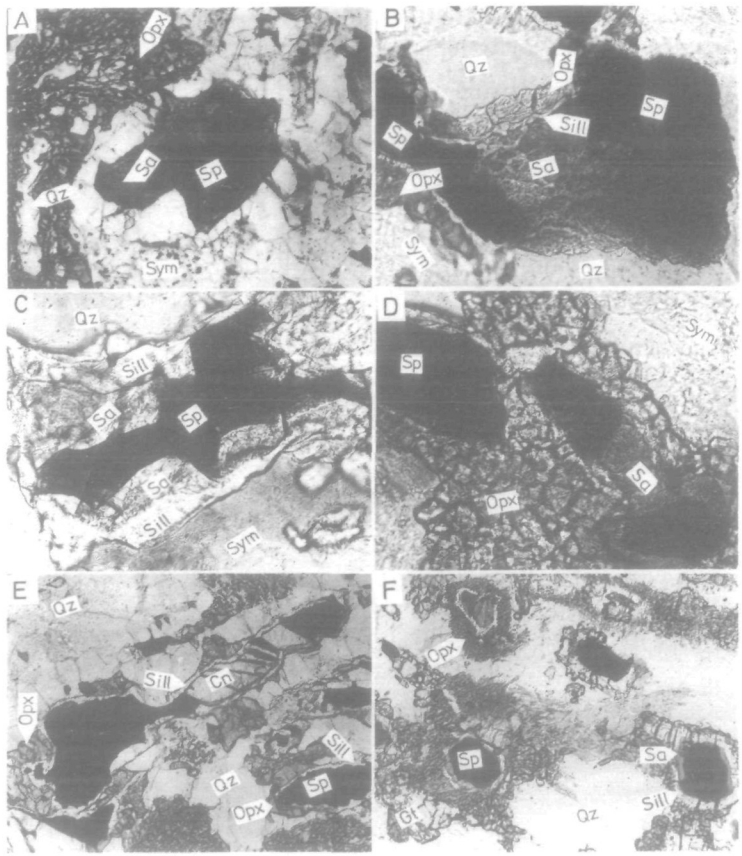

FIG. 2. Photomicrographs showing the reaction coronas in rock type A-2. (A) Overgrowth of sapphirine on spinel. Both sapphirine and spinel (partially) are in grain contact with quartz. Sample no. 321, rock type A-2-2. Long dimension = 0·52 mm. Plane polarized light. (B) Sapphirine and spinel partially separated from quartz by a reaction corona of sillimanite and orthopyroxene (reaction 6, Table 2). Cd–Kf–Qz–Opx symplectite (Sym) are present in the groundmass in the top right and bottom left. Sample no. 323, rock type A-2-1. Long dimension = 0·32 mm. Plane polarized light. (C) Spinel and sapphirine are completely separated from quartz, reaction corona Sp–Sa–Sill (reaction 1, Table 2). Sample no. 258 A, rock type A-2-1. Long dimension = 0·21 mm. Plane polarized light. (D) Spinel and sapphirine are separated from quartz in the matrix by reaction corona of orthopyroxene, reaction corona Sp–Sa–Opx (reaction 2). Sample no. 256, rock type A-2-1. Long dimension = 0·32 mm. Plane polarized light. (E) Reaction corona (Ilmeno-hem/Hem-ilm–Sp ± Cn)–Sill–Opx (reaction 7 and 19) in sample no. 321, rock type A-2-2. Long dimension = 0·87 mm. Plane polarized light. (F) Reaction corona Sp–Sa–Sill–Gt ± Qz (reactions 11, 16), Sp–Sa–Sill–Opx ± Qz (reactions 1, 12) and Sp–Sa–Sill–Opx–Gt (reaction 14). Sample no. 244, rock type A-2-3. Long dimension = 1·26 mm. Plane polarized light.

sequence of development of the reaction textures during metamorphism is best documented by the textural relations in rock type A-2-3.

Reaction textures of the Early Stage

These are characterized by polymineralic coronas. Sapphirine and spinel were in equilibrium with quartz during the thermal peak of metamorphism (Fig. 2A). Later, sapphirine and spinel in grain contact with quartz were partially rimmed successively by sillimanite and orthopyroxene (Figs. 2B and 4A), while spinel was completely separated from

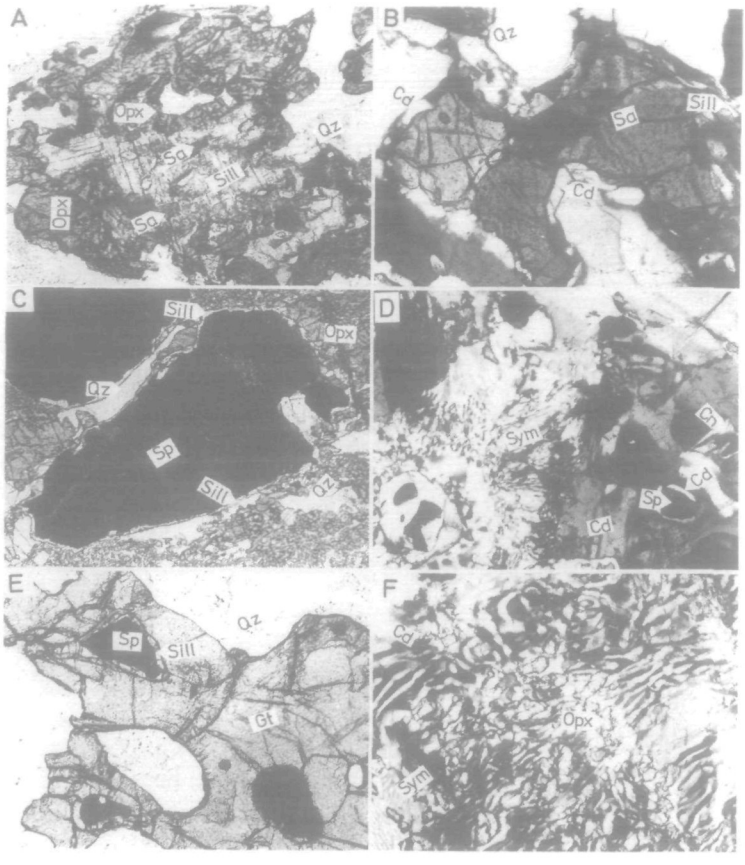

FIG. 3. Photomicrographs showing the coronas and other reaction textures in the rock type A-1-2, B, and C. (A) Sapphirine inclusions in sillimanite rimmed by orthopyroxene, reaction corona Sa–Sill–Opx (reaction 8). Sample no. 249, rock type A-1-2. Long dimension = 0·72 mm. Plane polarized light. (B) Sapphirine separated from quartz by a rim of sillimanite (right) and cordierite (bottom and left), reaction corona Sa–Sill–Cd (reaction 4). Sample no. 249, rock type A-1-2. Long dimension = 0·52 mm. Crossed polarized light. (C) Reaction corona Sp–Sill–Opx (reaction 7) separating spinel from quartz in the rock type B-1-1 (sample no. 339). Long dimension = 0·94 mmm. Plane polarized light. (D) Spinel (± Cn) separated from quartz by a rim of cordierite (reaction 17 and 19), in sample no. H-2 (rock type B-1-2). Long dimension = 0·82 mm. Crossed polarized light. (E) Spinel separated from quartz by a reaction corona of sillimanite and garnet, reaction corona Sp–Sill–Gt (reaction 3). Sample no. 332 (rock type B-2-1). Long dimension = 0·52 mm. Plane polarized light. (F) Cordierite–potash-feldspar–quartz–orthopyroxene symplectite, which possibly formed from the breakdown of osumilite in sample no. 259, rock type C-1. Similar symplectites also occur in the rock types A and B. Long dimension = 0·82 mm. Crossed polarized light.

quartz by sapphirine + sillimanite (Fig. 2C), sapphirine + orthopyroxene (Fig. 2D), sillimanite + orthopyroxene (Fig. 2E), sapphirine + sillimanite + garnet (Fig. 4B), sapphirine + sillimanite + orthopyroxene (Fig. 2F), sapphirine + sillimanite + garnet (Fig. 2F). The common occurrence of ilmeno-hematite/hemo-ilmenite in association with spinel, with or without corundum, in the core of the coronas (Fig. 2E) suggests highly oxidizing conditions during the early stage of their formation. This includes the corona types: (Sp–Ilmeno-hem–Cn)–Sill, (Sp–Ilmeno-hem)–Sill, (Sp–Ilmeno-hem)–Sill–Opx and (Sp–Ilmeno-hem–Cn)–Sill–Opx. The orthopyroxene and garnet (Opx II and Gt II) in the reaction coronas differ from the coarse prisms of orthopyroxene and garnet (Opx I and Gt I) present in the matrix, in that Opx

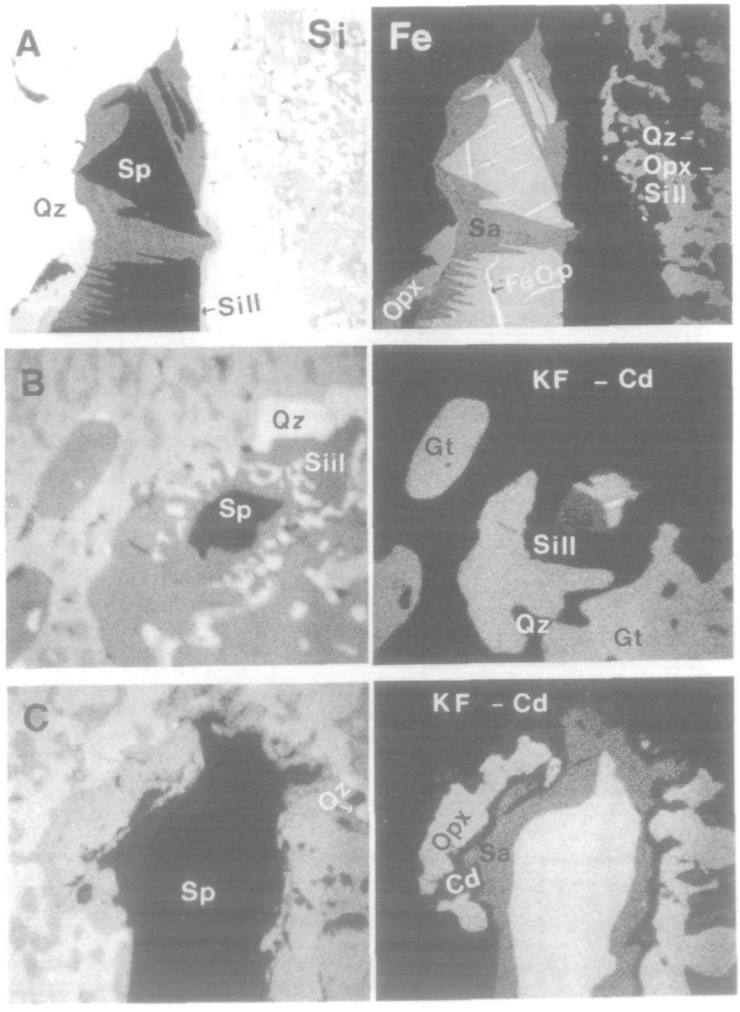

FIG. 4. X-ray K_α distribution photographs for the elements Si and Fe. (A) Reaction corona Sp–Sa–Sill–Opx–Qz (reaction 6). Note sapphirine and also spinel are in grain contact with quartz. Sample no. 321 (rock type A-2-2). (B) Reaction corona Sp–Sa–Sill–Gt–Qz (reaction 11) in the matrix of Cd–Kf–Qz–Opx symplectites. Sample no 244 (rock type A-2-3). (C) Reaction corona Sp–Sa–Cd–Opx (reaction 18) in the matrix of Cd–Kf–Qz–Opx symplectites in sample no. 265 (rock type A-2-3).

II and Gt II are fine-grained prisms and small granular aggregates respectively. Similar Opx II also occurs as finger-like trails within the (Cd–Kf–Qz–Opx) symplectite and also as overgrowths around coarse orthopyroxene.

Reaction textures of the Middle Stage

These include reactions which did not result in coronas, but in other reaction textures. For example, cordierite and potash feldspar in the fine-grained (Cd–Kf–Qz–Opx) symplectites

recrystallized to coarse aggregates. This cordierite contains linear trails of sillimanite and elongated quartz and overprints the fabric of the quartzofeldspathic groundmass. In samples containing coarse porphyroblasts of cordierite in grain contact with orthopyroxene or garnet, there is a tendency for orthopyroxene and garnet to be separated from quartz or sillimanite by a reaction zone of cordierite. Garnet similar to Gt II occurs as small idioblasts commonly symplectitically intergrown with quartz, as overgrowths around coarse garnet (Gt I) and orthopyroxene (Opx I), and also within the (Cd–Kf–Qz–Opx) symplectite. Coarse garnet similar to Gt I occurs in many samples and contains inclusions of spinel, sapphirine and the reaction coronas related to the reaction textures of the Early Stage. Presumably these are recrystallized garnet of a later generation.

Reaction textures of the Late Stage

In all the assemblages of type A, B, and C rocks, variable amounts of retrograde biotite or biotite + quartz symplectite replace orthopyroxene, garnet, cordierite, and (Cd–Kf–Qz–Opx) symplectite.

Not all the rocks of type A-2 preserve the reaction textures of all three Stages. For example A-2-1 and A-2-2 rocks mostly show evidence for reaction textures of the Early and Late Stages.

The rock type A-1 contains the coronas and other reaction textures of Early, Middle and Late Stages. As these rocks are devoid of spinel, the reaction coronas are different from those of the A-2 rocks. These are characterized by the corona types Sa–Sill–Opx (Fig. 3A), Sa–Sill–Cd (Fig. 3B), Sa–Cd–Opx and Sa–Sill–Opx–Gt. Besides the reaction textures of the Middle Stage given for the A-2-3 rocks, these also contain symplectitic intergrowths of sapphirine + cordierite between orthopyroxene and sillimanite.

Type B: spinel-bearing but sapphirine-free

Without garnet (B-1)

B-1-1: Opx, Sill, Kf, Qz, Plag, Sp, (Cd–Kf–Qz–Opx) symplectite and Bio
B-1-2: Opx, Sill, Qz, Kf, Cd, Sp, Bio, (Cd–Kf–Qz–Opx) symplectite ± Plag

With garnet (B-2)

B-2-1: Gt, Sp, Opx, Qz, Sill, Kf, Plag (An_{39}) and Bio
B-2-2: Gt, Bio, Sp, Qz, Sill, Kf, (Cd–Kf–Qz) symplectite, Cd and Plag (An_{30})

Minor constituents also include the minerals listed for type A rocks (see above).

The textural relations of garnet, orthopyroxene, sillimanite, and (Cd–Kf–Qz–Opx) symplectites in this rock type are similar to those of the type A rocks. In a sample of type B-1, spinel occurs in textural equilibrium with quartz. In most samples, however, it is separated from quartz by coronas, viz. Sp–Sill–Opx (in B-1-1, B-1-2, and B-2-1, Fig. 3C), Sp–Sill–Gt (in B-2-1, Fig. 3E) and Sp–Cd (in B-1-2, Fig. 3D). Highly oxidizing conditions during the formation of the coronas in the Early Stage are evident from the presence of (Sp–Ilmeno-hem)–Sill–Opx and (Sp–Ilmeno-hem–Cn)–Cd coronas. The types B-1-1 and B-2-1 display reaction textures of the Early and Late Stages only, B-1-2 of all three Stages and B-2-2 only of the Late Stage.

Type C: sapphirine and spinel-free

The textural relations in charnockite, khondalite, leptynite and mafic granulite are not included, in this section.

C-1: Opx, Sill, Qz, Kf, (Cd–Kf–Qz–Opx) symplectite, Bio + Gt ± Cd ± Plag (An_{72})
C-2: Bio, Sill, Kf, Qz, (Cd–Kf–Qz) symplectite Plag ± Gt ± Cd

Minor amounts of zircon, apatite, rutile, magnetite, and ilmenite are also present.

No reaction coronas are present and thus these rocks lack reaction textures of the Early Stage, except for the symplectites believed to be a breakdown product of osumilite. The textural relations of the minerals in the type C rocks are similar to those described for type A. The C-1 assemblages display reaction textures of the Middle as well as the Late Stage. The imprints of the Late Stage are much more common in type C assemblages than in type A and B assemblages. On the other hand, C-2 rocks preserve only the textures of the Late Stage, for example garnet isolated from potash feldspar by a zone of quartz and randomly oriented sillimanite intergrown with biotite. The ubiquitous presence of magnetite and ilmenite, and the rarity or absence of ilmenite–hematite intergrowths in the type-C rocks suggest less oxidizing conditions during the formation of these, as compared to types A and B.

The variety of reaction textures in the different rock types and reactions inferred from them are summarized in Table 2. Further discussion is deferred to the section on chemographic relationships and metamorphic reactions.

MINERAL CHEMISTRY

Microprobe analyses of sapphirine (Table 3) yield structural formulae in good agreement with the general formula $M_7(M)O_2(T_6O_{18})$ (Moore, 1969), when Fe^{3+} is calculated from stoichiometry. Minor Cr_2O_3 is present in some sapphirine (up to 0·89 wt. per cent Cr_2O_3). The sapphirine shows solid solution according to the substitution $(Mg, Fe^{2+}) + Si = 2(Al, Fe^{3+}, Cr)$. Sapphirine compositions lie between the $2(Mg, Fe)O:2R_2O_3:SiO_2$ (2:2:1) and the $7(Mg, Fe)O:9R_2O_3:3SiO_2$ (7:9:3) compositions, but lie generally nearer the latter (Fig. 5). Sapphirine grains coexisting with orthopyroxene have lower R_2O_3 than those not associated with orthopyroxene. The X_{Mg} (= Mg/(Mg + Fe)) in sapphirine ranges from 0·72 to 0·82, and the total iron contents (as FeO) up to 12·2 wt. per cent, the highest so far reported for sapphirine from sapphirine–quartz associations. Sapphirine in textural equilibrium with quartz contains more Fe^{3+} than most sapphirine in the rocks studied. It is richer in Fe^{3+} than sapphirine from the sapphirine–quartz granulites of Antarctica (Ellis *et al.*, 1980; Grew, 1980*a*, up to 0·13 atoms p.f.u.), and poorer in Fe^{3+} than the sapphirine from Wilson Lake (Higgins *et al.*, 1979, 0·47 atoms p.f.u.) and Peekskill, New York (Caporuscio & Morse, 1978, 0·65 atoms p.f.u.). No significant compositional zoning in individual crystals has been observed. However, the composition varies among individual grains and among grains from the different types of coronas. Examples are as follows: (a) sapphirine overgrowths on spinel coexisting with quartz have a higher X_{Mg} than sapphirine in the Sp–Sa–Sill–Opx coronas; (b) sapphirine in the Sp–Sa–Sill–Gt coronas has lower X_{Mg} and Fe^{3+} than the sapphirine from the Sp–Sa–Sill–Opx coronas; (c) sapphirine from the spinel-free type A-1-1 assemblage has higher X_{Mg} than spinel-bearing type A-2 assemblages. The sapphirine from the A-1-1 rocks occurs in corona types Sa–Sill–Opx, Sa–Sill–Cd and Sa–Cd–Opx.

Spinels are essentially solid solutions of spinel–hercynite. X_{Mg} is rather high in the type-A assemblages (0·44–0·62), where spinel is associated with sapphirine, but distinctly lower (0·31–0·39) in the type-B assemblages which are devoid of sapphirine (Table 3). The Fe^{3+}-content, calculated from the stoichiometry, ranges from 0·04 to 0·20 atoms p.f.u., based on 6 cations. Some of the spinels contain Cr_2O_3, ZnO, and rarely NiO up to 1·96, 2·90, and 0·53 wt. per cent respectively. Spinel always has higher Cr_2O_3-contents than associated sapphirine. The X_{Mg} and the Fe^{3+} content of spinel from the Sp–Sa–Sill–Gt coronas are lower than these from the Sp–Sa–Sill–Opx coronas.

TABLE 2

Reactions deduced from coronas and other reaction textures in different rock types. The type of corona present in the different rock types is shown by horizontal lines. The matrix of the reaction coronas consists of quartz, K-feldspar and (Cd–Kf–Qz–Opx) symplectite.

React. no.	*Reactions*	*Corona types*	*No. of samples in which the corona type is present*	*Fig. nos*	*Sa-bearing* *A-1-1*	*A-1-2*	*A-2-1*	*A-2-2*	*A-2-3*	*Sp-bearing but Sa-free* *B-1-1*	*B-1-2*	*B-2-1*	*B-2-2*	*Sp–Sa-free* *C-1*	*C-2*
Early Stage		*Core-->rim*													
1.	Sp + Sill + Qz = Sa	Sp–Sa–Sill	3	2C											
2.	Sp + Qz = Opx + Sa	Sp–Sa–Opx	5	2D											
3.	Sp + Qz = Gt + Sill	Sp–Sill–Gt	5	3E											
4.	Sa + Qz = Cd + Sill	Sa–Sill–Cd	2	3B											
5.	Sa + Opx + Qz = Cd	Sa–Cd–Opx	2	—											
6.	Sp + Sa + Qz = Opx + Sill	Sp–Sa–Sill–Opx–Qz	3	2B, 2F 4A											
7.	Sp + Qz = Opx + Sill	Sp–Sill–Opx	7	2E, 3C											
8.	Sa + Qz = Opx + Sill	Sa–Sill–Opx	6	3A											
11.	Sp + Qz = Gt + Sa + Sill	Sp–Sa–Sill–Gt–Qz	4	2F, 4B											
12.	Sp + Opx + Sill = Sa	Sp–Sa–Sill–Opx	4	—											
13.	Sp + Opx + Sill = Gt	Sp–Sill–Opx–Gt	2	—											
14.	Opx + Sill + Sp = Sa + Gt	Sp–Sa–Sill–Opx–Gt	1	—											
15.	Sa + Opx + Sill = Gt	Sa–Sill–Opx–Gt	3	—											
16.	Sp + Gt + Sill = Sa	Sp–Sa–Sill–Gt	4	—											
17.	Sp + Qz = Cd	Sp–Cd	3	—											
18.	Cd + Sp = Sa + Opx	Sp–Sa–Cd–Opx	1	4C											
Middle Stage															
22.	Opx + Sill + Qz = Cd	corona absent													
23.	Opx + Sill = Gt + Qz														
24.	Gt + Sill + Qz = Cd														
25.	Cd + Opx = Gt + Qz														
26.	Opx + Sill = Sa + Cd														
Late Stage															
27.	Cd + Opx + Kf + V = Bio + Qz	corona absent													
28.	Gt + Cd + Kf + V = Bio + Sill + Qz														
29.	Opx + Kf + Gt + V = Bio + Qz														
30.	Gt + Kf + V = Bio + Sill + Qz														

TABLE 3

Representative microprobe analyses of sapphirine and spinel

	Sapphirine						Spinel					
Rock-type	*A-1-1*	*A-2-1*	*A-2-2*	*A-2-3*	*A-2-2*	*A-2-2*	*A-2-1*	*A-2-2*	*A-2-3*	*A-2-2*	*B-1-2*	*B-2-2*
Sample no.	*17 II*	*303*	*302*	*320*	*321†*	*321*	*303*	*302*	*320*	*321*	*258*	*252*
	weight per cent											
SiO_2	13·1	13·6	12·4	13·3	12·7	12·2	—	—	—	—	—	—
Al_2O_3	63·0	58·7	61·3	61·3	61·0	61·5	60·1	61·5	61·4	60·6	60·4	59·2
Cr_2O_3	—	—	0·27	—	—	0·39	—	0·83	—	0·91	—	—
FeO*	7·89	12·2	9·75	10·3	10·5	10·6	26·6	24 5	26·6	25·7	29·6	31·5
MnO	0·05	0·26	—	—	—	—	0·53	0·04	—	0·44	0·50	0·68
MgO	16·4	14·7	15·2	16·0	15·7	15·3	11·4	13·4	11·5	12·1	9·67	7·62
ZnO	—	—	—	—	—	—	1·50	0·25	1 10	—	—	1·00
Total	100·44	99·46	98·92	100·9	99·9	99·99	100·13	100·52	100·6	99·75	100·17	100·00
	Formulae based on 14 cations						*Formulae based on 6 cations*					
Si	1·545	1·656	1·501	1 577	1·525	1·460	—	—	—	—	—	—
Al	8·781	8·410	8·743	8 579	8·622	8·701	3·805	3·822	3·859	3·827	3·855	3·849
Cr	—	—	0·026	—	—	0·037	—	0·035	—	0·040	—	—
Fe^{3+}	0·129	0·276	0·228	0·266	0·327	0·341	0·197	0·141	0·143	0·131	0·145	0·149
Fe^{2+}	0·659	0·960	0·757	0·753	0·726	0·719	0·998	0·940	1·042	1·021	1·196	1·303
Mn	0·005	0·027	—	—	—	—	0·024	0·002	—	0·020	0·023	0·032
Mg	2·885	2·671	2·745	2·826	2·802	2·744	0·916	1·051	0·912	0·962	0·781	0·627
Zn	—	—	—	—	—	—	0·059	0·010	0·043	—	—	—
X_{Mg}	0·814	0·730	0·784	0·790	0·794	0·793	0·472	0·528	0·467	0·480	0·391	0·325

* Total iron as FeO. Fe^{3+} calculated from stoichiometry.

† Sapphirine in contact with quartz. Fe^{3+} in sapphirine and spinel has been calculated from stoichiometry after normalizing the formulae to 14 and 6 cations respectively. In sapphirine $Fe^{3+} = Al^{IV} - (Al^{VI} + Cr)$ (present study) and in spinel-hercynite $Fe^{3+} = 16 - (2R^{2+} + 3R^{3+}$ cations) (Bohlen & Essene, 1977). For microprobe technique used for analyses refer to Raith *et al.* (1983). $X_{Mg} = Mg/(Mg + Fe^{2+})$.

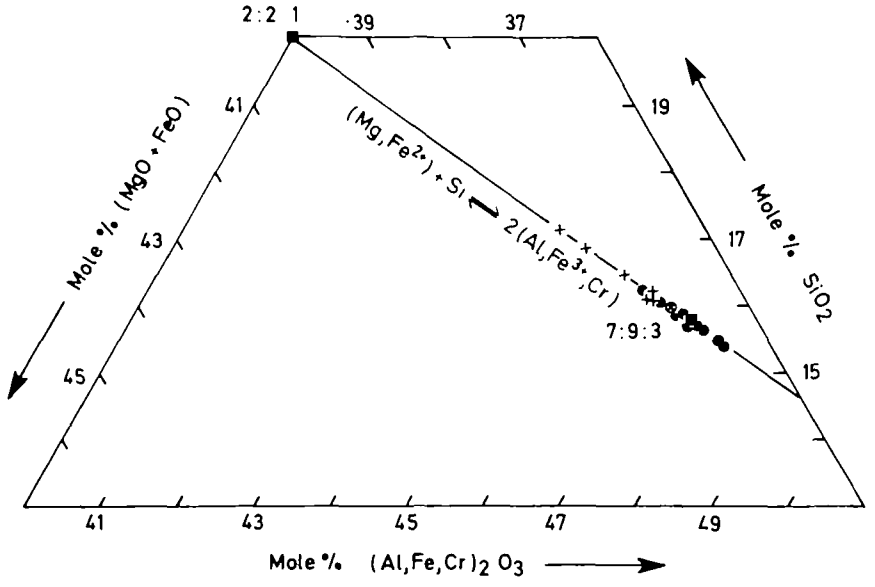

FIG. 5. Compositional variation of sapphirine in the Paderu area, projected onto the water-free basal plane (Mg, Fe) O–(Fe, Al, Cr)$_2$O$_3$–SiO$_2$. The numbers 2:2:1 and 7:9:3 (solid squares) are the molar proportions of (Mg, Fe) O:(Fe, Al, Cr)$_2$O$_3$:SiO$_2$. Crosses—sapphirine coexisting with orthopyroxene; circle with cross—sapphirine in textural equilibrium with quartz; solid circles—sapphirine coexisting with neither orthopyroxene nor quartz.

Garnets consist essentially of the almandine and pyrope components (46–66 and 25–52 mol per cent respectively, Table 4). Garnets in A-2 and C-1 assemblages have higher X_{Mg} (0·48 to 0·52 wt. per cent) than those in the type B-2 (0·29 to 0·43 wt. per cent). Coarse garnet porphyroblasts of the earlier generation are commonly zoned, with X_{Mg} decreasing from core to rim. The X_{Mg} is consistently lower in garnets from the garnet–quartz symplectites and reaction coronas.

Orthopyroxenes coexisting with sillimanite are aluminous, and contain up to 10·4 wt. per cent Al_2O_3 (Table 5). The coarse orthopyroxenes are zoned, and show a marked decrease of Al_2O_3 and a minor decrease of X_{Mg} from core to rim. Orthopyroxenes associated with the reaction coronas and the (Cd–Kf–Qz–Opx) symplectites have consistently lower Al_2O_3 compared with coarse orthopyroxenes from the same thin-section. The X_{Mg} of the orthopyroxenes ranges from 0·64 to 0·74 in rock types A-1, A-2, and C-1 and from 0·55 to 0·69 in B-1 and B-2.

Cordierites are essentially unzoned; X_{Mg} ranges from 0·84 to 0·88 in rock types A-1, A-2, and C, and from 0·78 to 0·83 in B-1 and B-2. The low analtyical sums (Table 6) suggest the presence of significant amounts of gaseous species (probably mostly CO_2, as indicated by the absence of Na_2O) in the structural channels.

X_{Mg} of biotites and phlogopites from the sillimanite–orthopyroxene assemblages (types A-1, A-2, B-1, B-2, and C, Table 6) ranges from 0·75 to 0·89. The variation in TiO_2 content, 1·16–4·9 wt. per cent TiO_2, may reflect re-equilibration during the retrograde episode. Sillimanite contains more Fe_2O_3 in the sapphirine- and spinel-bearing assemblages (types A and B, 0·73–1·52 wt. per cent) than sillimanite in the type C assemblages (0·52–0·56 wt. per cent). Relatively high contents of Fe_2O_3 in sillimanite are also reported from sapphirine–quartz rocks from Wilson Lake, Labwor, and Peekskill (1·2 to 1·7 wt. per cent, Caporuscio & Morse, 1978; Grew, 1980*b*). High Fe_2O_3 contents of sillimanite in the Paderu

TABLE 4

Representative microprobe analyses of garnet

Rock type	*A-2-2*	*A-2-3*	*A-2-2*	*B-2-2*		*C-1*
Sample no	*302*	*320*	*321*	*252 C*	*R†*	*259*
			weight per cent			
SiO_2	39·0	39·3	38·8	38·5	37·7	39·5
Al_2O_3	22·7	22·7	22·3	22·3	22·1	22·5
FeO*	23·6	23·4	23·6	26·6	31·1	22·8
MnO	0·46	0·62	0·62	1·01	1·42	0·98
MgO	13·3	14·2	13·3	11·3	7·55	13·3
CaO	0·38	0·32	0·23	0·88	1·06	0·75
Total	99·44	100·54	98·85	100·59	100·93	99·83
			Formulae based on 24 oxygens			
Si	5·913	5·887	5·924	5·866	5·874	5·953
Al	4·054	4·004	4·009	4·013	4·053	3·996
Fe^{2+}	2·983	2 927	3·009	3·394	4·056	2·872
Mn	0·059	0·079	0·080	0·131	0·187	0·125
Mg	2 991	3·163	3·012	2·580	1·753	2·981
Ca	0·062	0·051	0·038	0·144	0·177	0·121
X_{Mg}	0·501	0·519	0·500	0·432	0·302	0·509

* Total iron as Feo and Fe^{2+}.

† Garnet from garnet–quartz symplectite rimming core. C = core R = rim.

$X_{Mg} = Mg/(Mg + Fe^{2+})$. TiO_2 and Cr_2O_3 are below detection limit.

TABLE 5

Representative microprobe analyses of orthopyroxene

Rock type	*A-1-1*	*A-2-1*	*A-2-2*	*A-2-3*	*B-1-2*	*B-2-2*	*C-1*	*C-1*	*C-1*
Sample no.	*17 II*	*303*	*321*	*320*	*258*	*252*	*295*	*295†*	*259*
				weight per cent					
SiO_2	49·9	46·2	49·9	50·4	47·8	48·6	49·1	50·6	49·6
TiO_2	0·08	0·15	—	0·15	—	—	—	0·09	0·24
Al_2O_3	8·59	10·4	7·26	6·48	6·80	6·76	9·69	6·60	9·64
FeO*	16·8	21·1	18·7	17·1	25·5	26·0	19·7	20·2	17·1
MnO	0·14	0·43	0·23	—	0·60	0·65	0·27	0·17	—
MgO	24·6	20·2	23·6	24·7	18·9	17·9	22·0	22·2	23·6
Total	100·11	98·48	99·69	98·83	99·60	99·91	100·76	99·86	100·18
				Formulae based on 4 cations					
Si	1·798	1·732	1·822	1·847	1·808	1·844	1·785	1·860	1·792
Ti	0·002	0·004	—	0·004	—	0·302	—	0·003	0·006
Al	0·365	0·460	0·313	0·280	0·303	—	0·416	0·286	0·411
Fe^{3+}	0·036	0·068	0·044	0·019	0·081	0·011	0·014	—	—
Fe^{2+}	0·469	0·595	0·528	0·504	0·725	0·812	0·584	0·622	0·516
Mn	0·004	0·014	0·007	—	0·019	0·021	0·008	0·005	—
Mg	1·323	1·128	1·286	1·347	1·603	1·010	1·193	1·216	1·271
X_{Mg}	0·738	0·655	0·709	0·728	0·689	0·554	0·671	0·660	0·711

* Total iron as FeO. Fe^{3+} has been calculated by stoichiometry (Hamm & Vieten, 1971).

† Orthopyroxene associated with (Cd–Kf–Qz–Opx) symplectite.

area are consistent with high Fe^{3+} contents of associated sapphirine and spinel. In the type A rocks, corundum contains 0·94–1·32 wt. per cent Fe_2O_3 and *rutile* contains 0·62 wt. per cent FeO. Hemo-ilmenite (7·95–15·06 wt. per cent Fe_2O_3) and ilmeno-hematite (55·66–74 wt. per cent Fe_2O_3) from the type A-2 rocks contain up to 1·17 and 2·23 wt. per cent Cr_2O_3 and

TABLE 6

Representative microprobe analyses of cordierite and biotite/phlogopite

	Cordierite					*Biotite/Phlogopite*				
Rock type	*A-1-1*	*A-2-2*	*B-1-2*	*B-2-2*	*C-1*	*A-2-1*	*A-2-2*	*B-2-2*	*C-1*	*C-1*
Sample no	*17 II*	*320*	*258*	*252*	*259*	*303*	*302*	*252*	*259*	*295*
					weight per cent					
SiO_2	50·3	47·6	47·6	47·5	48·1	38·5	39·5	39·6	39·3	39·3
TiO_2	—	—	—	—	—	4·36	4·38	1·61	3·29	4·84
Al_2O_3	33·4	33·1	32·5	30·0	33·0	13·1	14·4	14·1	13·5	13·4
FeO*	2·75	3·71	5·14	5·48	3·91	8·17	6·05	5·29	7·83	9·73
MnO	0·03	—	—	0·24	0·18	—	—	—	—	0·02
MgO	11·8	12·5	12·2	11·6	11·9	19·5	21·3	22·5	19·5	17·4
K_2O	—	—	—	—	—	10·3	10·4	10·2	9·48	10·0
Anhydrous total	98·28	96·91	97·44	94·82	97·09	93·93	96·03	93·30	92·90	94·69
X_{Mg}	0·883	0·857	0·809	0·790	0·844	0·809	0·862	0·883	0·816	0·761

* Total iron as FeO.

F and Cl contents of biotites in the sample no. 302 are 1·5–1·7 and 0·15–0·17 wt. per cent and in the sample no. 252 are 1·0–2·5 and 0·05–0·08 wt. per cent respectively. Na_2O is below detection limit in cordierite and biotite/phlogopite.

MgO, respectively. Ilmenite from the type C rocks contains 0·91–0·92 wt. per cent MnO and 4·7–6·1 wt. per cent Fe_2O_3. X_{Mg} in the coexisting minerals decreases in the order cordierite > biotite > sapphirine > orthopyroxene > spinel > garnet core > garnet rim.

CHEMOGRAPHIC RELATIONSHIPS AND METAMORPHIC REACTIONS

The reaction coronas in the sapphirine- and spinel-bearing rocks suggest disequilibrium during metamorphic crystallization. However, in microscopic domains, the minerals in a corona may have attained local equilibrium. This may be further corroborated by the chemographic relationships.

The sapphirine- and spinel-bearing rocks provide an example of a multi-component and multi-phase system. The phase relations can be portrayed in the model system K_2O–FeO–MgO–Al_2O_3–SiO_2–H_2O (KFMASH). This can be further simplified by excluding the K_2O-bearing minerals osumilite, biotite, and K-feldspar from the discussion of the phase relationships. This is justified, because K-feldspar is ubiquitous and can thus be treated as an excess phase. Moreover osumilite is not preserved in these rocks and thus its composition can not be measured, while biotite and phlogopite are involved in metamorphic reactions mostly during the late retrogressive stage. Thus the phase relations can be discussed in the FeO–MgO–Al_2O_3–SiO_2–H_2O system (FMASH). It must be emphasized here that this system is also a simplification, because Fe^{3+} and Cr^{3+} are present in sapphirine and spinel, and Zn in spinel.

We shall begin our discussion by treating MgO + FeO, as well as $Al_2O_3 + Fe_2O_3 + Cr_2O_3$ as single components, in an (Mg, Fe)O–(Al, Fe, Cr)$_2O_3$–SiO_2–H_2O system (Fig. 6). Despite its limited applicability to complex natural systems, as evident from the intersecting tie lines, the different continuous Fe–Mg exchange reactions involved in the formation of the reaction coronas (Table 2) can be easily deduced from the dispositions of the tie lines.

In the FMASH system, the phase relations can be portrayed in projections from quartz and water onto the AFM plane (AFM projection), and from sillimanite and water onto the SiO_2–$FeAl_2O_4$–$MgAl_2O_4$ plane (Robinson & Jaffe, 1969). On the basis of the phase

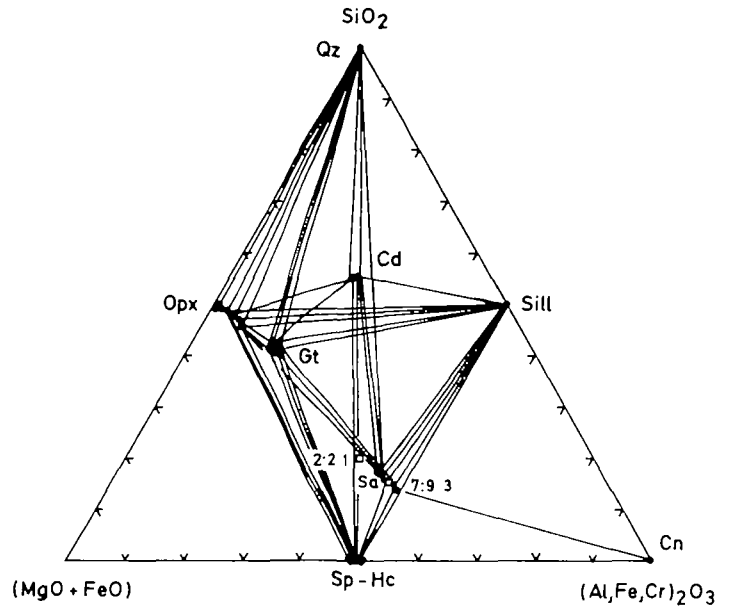

FIG. 6. Mineral compositions of the Paderu area plotted on the (Mg, Fe)O–(Fe, Al, Cr)$_2O_3$–SiO_2 projection. Crossed tie lines reflect variable fractionation of Mg and Fe^{2+}, as well as Al and Fe^{3+} among the phases.

compatibility relations in these projections, and the sequence of development of the reaction coronas (see above) it is possible to portray the metamorphic evolution of the rocks (Fig. 7). The variety of corona textures developed from the reactions involving Sa + Qz and Sp + Qz and the rarity of the assemblage Sa + Sp + Qz further corroborate the experimental data (Hensen & Green, 1971; Chatterjee & Schreyer, 1972; Newton, 1972), demonstrating a restricted *PT* stability field of the compatibility of sapphirine and spinel with quartz.

Spinel and sapphirine coexisted with quartz during the thermal peak of metamorphism (Fig. 7; rock types A-1, A-2, B-1, and B-2). During a later stage, spinel and sapphirine were isolated from quartz through continuous and discontinuous Fe^{2+}–Mg reactions. In the rock type A-2 (Sa–Sp-bearing), the earliest coronas are Sp–Sa–Sill and Sp–Sa–Opx (see the respective divariant three phase field in Fig. 7; A-1 and A-2). These corona-types presumably formed by the continuous Fe^{2+}–Mg reactions

$$\text{Sp} + \text{Sill} + \text{Qz} \rightleftharpoons \text{Sa} \quad (1)$$

$$\text{Sp} + \text{Qz} \rightleftharpoons \text{Opx} + \text{Sa}. \quad (2)$$

Reaction (1) is evident from Fig. 6, in which the sapphirine composition lies in the three-phase field Sp–Sill–Qz, and reaction (2) from the intersection of the Sp–Qz and Sa–Opx joins (Fig. 6). In the Mg-poor bulk compositions (rock type-B, Sp-bearing but Sa-free) the Sp–Sill–Gt corona (Fig. 3E) (three-phase field of Sp–Gt ± Sill ± Qz, Fig. 7; A-1 and A-2) is due to the reaction

$$\text{Sp} + \text{Qz} \rightleftharpoons \text{Gt} + \text{Sill}. \quad (3)$$

Reaction (3) is evident from the crossing of the Sp–Qz and Gt + Sill joins (Fig. 6). In the Mg-rich bulk compositions (rock type A-1, Sa-bearing but Sp-free) the reaction coronas Sa–Sill–Cd (Fig. 3B) and Sa–Cd–Opx (see the respective three phase fields in Fig. 7; A-1 and

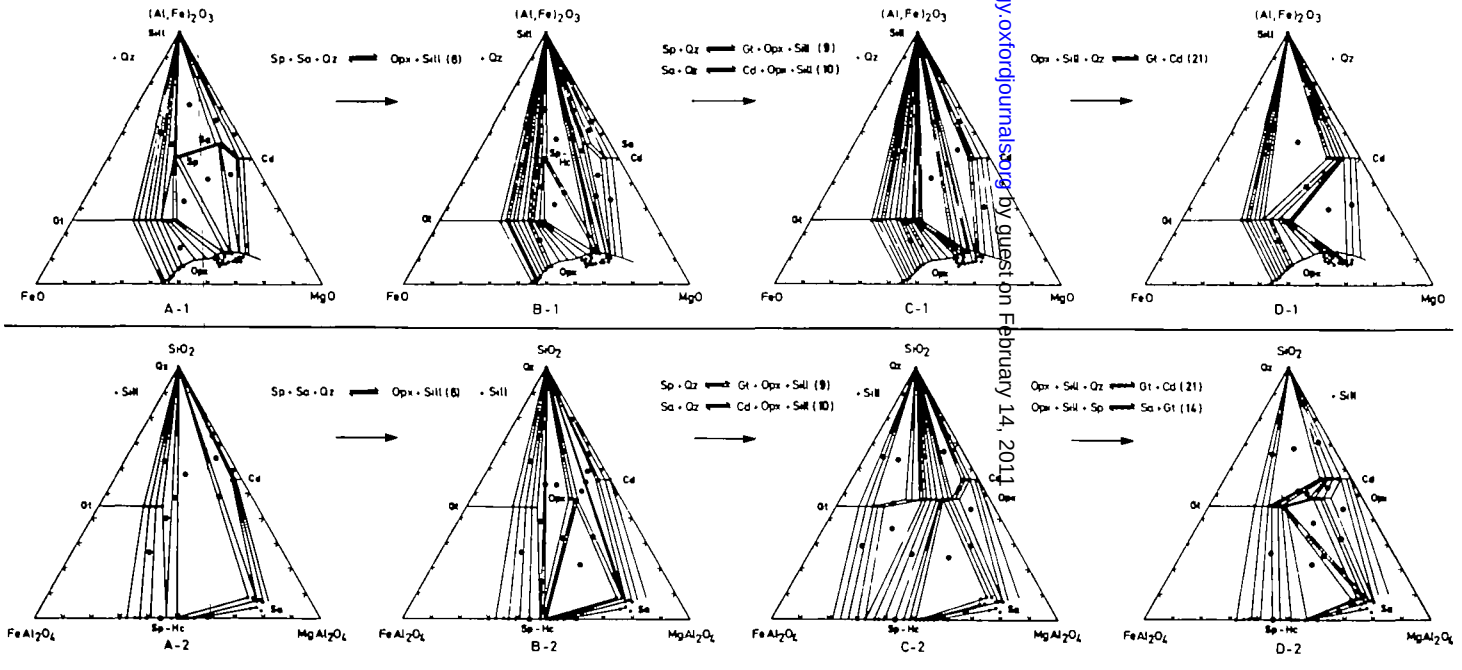

FIG. 7. A/1, B/1, C/1, and D/1: AFM projections from quartz, showing the sequence of reactions and changes in topology deduced from the textural relationships and compatibility relations of the mineral phases.

A/2, B/2, C/2, and D/2: Same as above, depicted in the projection from sillimanite onto the SiO_2–$FeAl_2O_4$–$MgAl_2O_4$ plane (Robinson & Jaffe, 1969).

Mineral compositions (small dots) and the tie lines connecting the coexisting minerals are shown for the different rock types. Large dots indicate the observed two-phase and three-phase mineral assemblages.

A-2) are related to reactions (4) and (5), which may be deduced from Fig. 6:

$$Sa + Qz \rightleftharpoons Cd + Sill \quad (4)$$

$$Sa + Opx + Qz \rightleftharpoons Cd. \quad (5)$$

The intersection of the two-phase field Sp–Sa by Opx–Sill in the AFM projection (Fig. 7; rock type A-1 and B-1), and the development of Opx–Sp, Opx–Sa and Opx–Qz joins within the three-phase field Sp–Sa–Qz in the sillimanite projection (Fig. 7; A-2 and B-2) are related to the discontinuous reaction

$$Sp + Sa + Qz \rightleftharpoons Opx + Sill. \quad (6)$$

The textural evidence for reaction (6) is the corona type Sp–Sa–Sill–Opx–Qz (Figs. 2B; 2F, and 4A) in the A-2-3 assemblage. The product minerals and two of the three reactants of reaction (6) constitute stable divariant assemblages. Due to the appearance of the Opx–Sill join, the continuous Fe^{2+}–Mg exchange reactions

$$Sp + Qz \rightleftharpoons Opx + Sill \quad (7)$$

$$Sa + Qz \rightleftharpoons Opx + Sill \quad (8)$$

will occur in the respective three-phase fields (Fig. 7; B-1 and B-2). The corona types Sp–Sill–Opx (Figs. 2E and 3C) and Sa–Sill–Opx (Fig. 3A) are textural evidence of reactions (7) and (8), respectively.

At a later stage, spinel and sapphirine became incompatible with quartz, presumably due to the discontinuous reactions

$$Sp + Qz \rightleftharpoons Gt + Opx + Sill \quad (9)$$

$$Sa + Qz \rightleftharpoons Opx + Cd + Sill \quad (10)$$

$$Sp + Qz \rightleftharpoons Gt + Sill + Sa. \quad (11)$$

Reactions (9) and (10) are evident, from the plot of spinel and sapphirine compositions within the three-phase fields of Gt–Opx–Sill and Cd–Opx–Sill in the AFM projection (Fig. 7; B-1 and C-1) and the intersections of the Sp–Qz and Sa–Qz joins with the Gt–Opx and Cd–Opx joins in the sillimanite projection (Fig. 7; rock type B-2 and C-2). Reaction (11) is documented by corona type Sp–Sa–Sill–Gt–Qz (Figs. 4B and 2F). The topology of the AFM projection related to this reaction is shown in Fig. 8. Because of reactions (9), (10) and (11), spinel and sapphirine were not in equilibrium with quartz, and therefore further development of coronas took place through reactions in silica-undersaturated bulk compositions (Fig. 7; B-2 and C-2). These include the corona types Sp–Sa–Sill–Opx (reaction 12) and Sp–Sill–Opx–Gt (reaction 13)

$$Sp + Opx + Sill \rightleftharpoons Sa \quad (12)$$

$$Sp + Opx + Sill \rightleftharpoons Gt. \quad (13)$$

The intersection of the Opx–Sp join by Gt–Sa (Fig. 7; rock type C-2 and D-2) is due to the discontinuous reaction

$$Opx + Sill + Sp \rightleftharpoons Gt + Sa. \quad (14)$$

The texture documenting reaction (14) is the corona type Sp–Sa–Sill–Opx–Gt. The corona types Sa–Sill–Opx–Gt and Sp–Sa–Sill–Gt were formed in the three-phase fields Sa–Opx–Gt and Sa–Sp–Gt in the sillimanite projection (Fig. 7; D-2) through the Fe^{2+}–Mg continuous

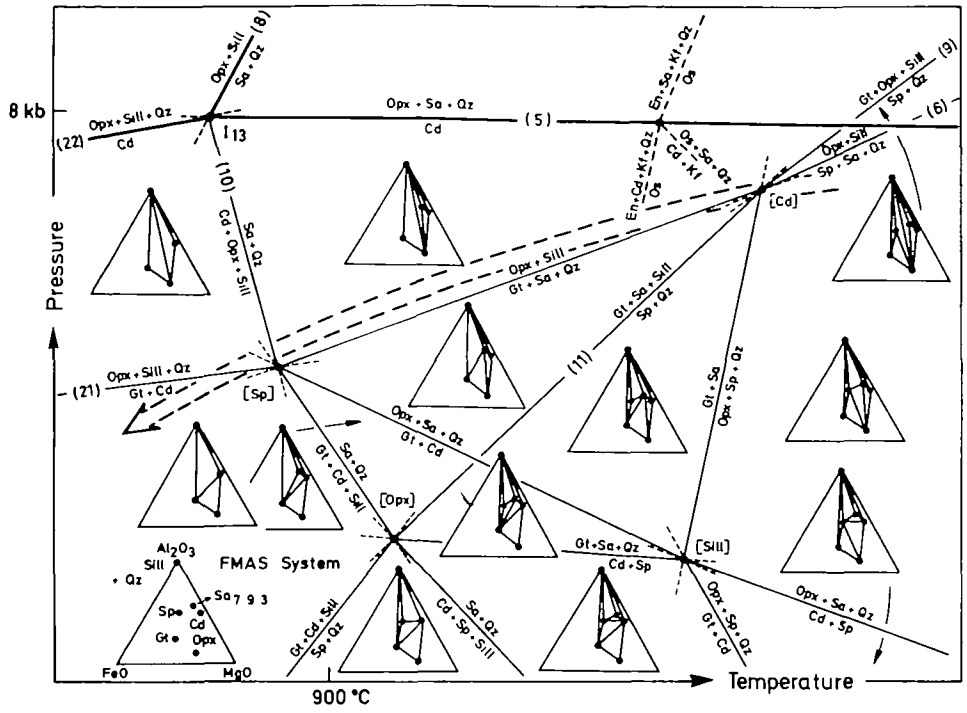

FIG. 8. Petrogenetic *PT* grid in the FMAS system, based on the experimental data of Hensen & Green (1971). The invariant point I_{13} and the univariant reactions (heavy lines) are based on the experimental data of Schreyer & Seifert (1969) and Newton (1972) for the MAS system. Osumilite breakdown reactions (dashed lines, Ellis *et al.*, 1980) for the KMAS system are also shown. The inferred *PT* trajectory is depicted by a dashed arrow. En-Enstatite. For the other mineral abbreviations refer to the section on textural relations. Numbers in parentheses correspond to those given in Table 2.

exchange reactions

$$\text{Sa} + \text{Opx} + \text{Sill} \rightleftharpoons \text{Gt} \tag{15}$$

$$\text{Sp} + \text{Gt} + \text{Sill} \rightleftharpoons \text{Sa}. \tag{16}$$

Other reaction coronas are Sp–Cd (Fig. 3D) in rock type B-1-2 and Sp–Sa–Cd–Opx (Fig. 4C) in type A-2, which are related to the reactions

$$\text{Sp} + \text{Qz} \rightleftharpoons \text{Cd} \tag{17}$$

$$\text{Cd} + \text{Sp} \rightleftharpoons \text{Sa} + \text{Opx}. \tag{18}$$

These reactions are not consistent with the topology of the AFM and sillimanite projection portrayed in Fig. 7 and are discussed in the next section (see below).

The coexistence of all the reactants and products of reactions (6), (11), and (14) in the coronas suggests that these univariant reactions become divariant due to incorporation of the additional component Fe_2O_3.

The common occurrence of ilmeno-hematite/hemo-ilmenite in association with spinel, with or without corundum, in the cores of the coronas (Fig. 2E) suggests the prevalence of highly oxidizing conditions during the Early Stage of their formation. The oxidation reactions may be

$$\text{Sp}_{ss}(1) + \text{Ru} + \text{Qz} + \text{O}_2 \rightleftharpoons \text{Sp}_{ss}(2) + \text{Ilmeno-hem} + \text{Cn} \tag{19}$$

$$\text{Sp}_{ss}(1) + \text{Ru} + \text{Qz} + \text{O}_2 \rightleftharpoons \text{Sp}_{ss}(2) + \text{Sill} + \text{Ilmeno-hem}. \tag{20}$$

Rutile as a reactant in reactions (19) and (20) is evident from its occurrence together with spinel and sapphirine in the cores of coronas in the less oxidized rocks. $Sp_{ss}(1)$ has a higher Fe^{2+}/Mg ratio than $Sp_{ss}(2)$. The corona types related to the above oxidation reactions are: (Sp–Ilmeno-hem–Cn)–Sill (reactions 19 and 20), (Sp–Ilmeno-hem)–Sill (reaction 20), (Sp–Ilmeno-hem–Cn)–Sill–Opx (reactions 7, 19, and 20, Fig. 2E), and (Sp–Ilmeno-hem–Cn)-Cd (reactions 17 and 19, Fig. 3D).

With the incompatibility of Sa + Qz and Sp + Qz, the reactions in the silica-saturated domains will occur without involving Sa and Sp. The intersection of the Opx–Sill and Opx–Qz fields with the Gt–Cd join in the AFM (Fig. 7; C-1 and D-1) and sillimanite projections (Fig. 7; C-2 and D-2), respectively, may be attributed to a discontinuous reaction

$$\text{Opx} + \text{Sill} + \text{Qz} \rightleftharpoons \text{Gt} + \text{Cd} \tag{21}$$

The continuous Fe^{2+}–Mg exchange reactions preceding and also following the completion of reaction (21) did not result in coronas, but in other reaction textures. These reactions in the three-phase fields Opx–Cd–Sill, Opx–Gt–Sill (Fig. 7; rock type C-1), Gt–Cd–Sill and Gt–Cd–Opx (Fig. 7; D-1) of the AFM projection include

$$\text{Opx} + \text{Sill} + \text{Qz} \rightleftharpoons \text{Cd} \tag{22}$$

$$\text{Opx} + \text{Sill} \rightleftharpoons \text{Gt} + \text{Qz} \tag{23}$$

$$\text{Gt} + \text{Sill} + \text{Qz} \rightleftharpoons \text{Cd} \tag{24}$$

$$\text{Cd} + \text{Opx} \rightleftharpoons \text{Gt} + \text{Qz}. \tag{25}$$

The textural evidence for reactions (22) and (24) are the crystallization of coarse porphyroblasts of cordierite in association of Opx/Gt–Sill–Qz, the modal decrease or absence of one of the three reactant minerals (usually sillimanite or quartz), and resorption of orthopyroxene/garnet by cordierite. The occurrence of garnet + quartz symplectite, which tends to isolate Opx from Sill or Cd, suggests reactions (23) and (25). Besides the textural evidence for reactions (22) to (25), rock type A-1-1 also contains symplectitic intergrowths of Sa + Cd between Opx + Sill. This texture presumably developed by the reaction

$$\text{Opx} + \text{Sill} \rightleftharpoons \text{Sa} + \text{Cd} \tag{26}$$

In all the assemblages of the rock types A, B, and C, variable amounts of retrograde biotite, biotite and quartz symplectite, and fine needles of sillimanite intergrown with biotite replace orthopyroxene, garnet, cordierite, K-feldspar, and (Cd–Kf–Qz–Opx) symplectite. These textures may be attributed to the hydration reactions (27) to (30).

$$\text{Cd} + \text{Opx} + \text{Kf} + \text{V} \rightleftharpoons \text{Bio} + \text{Qz} \tag{27}$$

$$\text{Gt} + \text{Cd} + \text{Kf} + \text{V} \rightleftharpoons \text{Bio} + \text{Sill} + \text{Qz} \tag{28}$$

$$\text{Opx} + \text{Kf} + \text{Gt} + \text{V} \rightleftharpoons \text{Bio} + \text{Qz} \tag{29}$$

$$\text{Gt} + \text{Kf} + \text{V} \rightleftharpoons \text{Bio} + \text{Sill} + \text{Qz}. \tag{30}$$

PETROGENETIC GRIDS AND *P–T–X* RELATIONSHIPS

A petrogenetic PT *grid for the FMAS system*

Based on the experimental data of Hensen & Green (1971), such a grid is shown in Fig. 8. The grid includes the invariant point I_{13} (Schreyer & Seifert, 1969), involving the phases Sa–Cd–Opx–Qz–Sill in MAS, and the osumilite breakdown reactions (Ellis *et al.*, 1980) in KMAS. The invariant point I_{13} is metastable in the MASH system, because of the formation

of melt at 1000 °C and $P > 10$ kb (Chatterjee & Schreyer, 1972; Newton, 1972). According to Newton (1972), the invariant point I_{13} (with Sa 2:2:1) is stable under the nearly anhydrous conditions of the granulite facies (800 °C/8 kb). With $Mg = Fe^{2+}$ substitution, the invariant point I_{13} shifts to lower pressures relative to the MAS system (Hensen & Green, 1971).

In the *PT* grid of the FMAS system, the relative positions of the invariant points [Sp], [Opx] and [Sill] and the dP/dT slopes of the univariant reactions (except the (Sa) reaction at the invariant point [Sp], cf. Newton, 1972) are based on the experimental data of Hensen & Green (1971) in the FMASH system. Sapphirine composition has been taken as 7:9:3 for constructing the grid, because it is closer to compositions of naturally occurring sapphirines than the 2:2:1 composition (Hensen & Green, 1971) inferred to be stable in the FMASH and MASH systems. Hensen (1971) considered the invariant points [Gt] and [Sa] to be metastable from experimental evidence and restrictions imposed by Schreinemakers rules. Hensen (1971) postulated that the invariant point [Cd] could be stable if the Cd-absent reactions emerging from the invariant points [Sp], [Opx] and [Sill] intersect at high pressures. On the other hand, if the reactions diverge towards higher pressures, the [Cd] invariant point would be metastable (e.g., Grew, 1982). We have shown the invariant point [Cd] as stable (Fig. 8), which is implied by the continuous reactions inferred from the corona textures and by the discontinuous reactions postulated from the chemographic relationships. The *PT* trajectory can be inferred to have followed the course of decreasing *P* and *T* (retrograde) from the invariant points [Cd] to [Sp]. This is further corroborated from the estimated *PT*-conditions derived from the different models of geothermobarometry.

The sapphirine–spinel–quartz-bearing parageneses are suitable for estimating the *PT* conditions of metamorphism from recently calibrated anhydrous mineral equilibria. Temperature has been estimated at pressures of 6·5 kb (core) and 5 kb (rim) on the basis of the garnet–orthopyroxene Fe–Mg exchange equilibrium (number of samples given in parantheses): core compositions (17) 900 ± 60 °C and rim compositions (8) 760 ± 50 °C (Harley, 1984); core (17) 1000 ± 50°C, rim (8) 840 ± 60 °C (Sen & Bhattacharya, 1984). The latter probably overestimates temperature by at least 100 °C for these rocks.

Pressure has been estimated using the mean temperature of 900 and 760 °C (Harley, 1984) for the core and rim compositions, respectively: (a) alumina-content of orthopyroxene coexisting with garnet (Harley & Green, 1982): core (23) $7{\cdot}0 \pm 0{\cdot}9$ kb, rim (2) 4·4 kb; (b) garnet–sillimanite–quartz–rutile–ilmenite equilibrium (Bohlen et al., 1983*b*): core (16) $6{\cdot}5 \pm 0{\cdot}3$ kb, rim (3) $6{\cdot}0 \pm 0{\cdot}1$ kb; and (c) garnet–orthopyroxene–plagioclase–quartz equilibrium: core (8) $6{\cdot}8 \pm 0{\cdot}8$ kb, rim (2) $4{\cdot}5 \pm 0{\cdot}3$ kb (Newton & Perkins, 1982); core (8) $5{\cdot}7 \pm 0{\cdot}6$ kb, rim (2) $5{\cdot}3 \pm 0{\cdot}7$ kb (Bohlen *et al.*, 1983*a*).

Mean values of temperature (Harley, 1984, garnet–orthopyroxene model only) and pressure estimated from the above models are 900 ± 60 °C/$6{\cdot}5 \pm 0{\cdot}7$ kb (core) and 760 ± 50 °C/$5{\cdot}0 \pm 0{\cdot}6$ kb (rim). This suggests a decrease of *P* and *T* in agreement with the retrograde trajectory qualitatively deduced from the *PT* grid (Fig. 8).

Nonetheless several questions remain unanswered from the *PT* petrogenetic grid:

(1) Could the invariant point [Cd] be metastable in the FMAS system (Hensen, 1971), but stable in natural sapphirine- and spinel-bearing parageneses due to Fe_2O_3 as an additional component? In the sapphirine–spinel-bearing rocks from Paderu and other areas, the continuous Fe–Mg exchange reactions related to the univariant reactions emerging from the invariant point [Cd] in the FMAS system are from assemblages in which high Fe^{3+} contents in sapphirine and spinel, as well as the opaque mineralogy, suggest metamorphic crystallization in an environment of high oxygen fugacity. Hensen (1986) has theoretically studied the influence of oxygen fugacity in the system Fe–Mg–Al–Si–O, involving the phases

cordierite, sapphirine, hypersthene, garnet, spinel, sillimanite, and quartz. He has proposed P–T petrogenetic grids in this system for low and high f_{O_2}. According to him, the [Cd] invariant point is metastable at low f_{O_2} (cf. Hensen, 1971) but becomes stable at high f_{O_2}.

(2) In some samples of these rocks from the Paderu area, Cd–Sp and Sp–Sa–Cd–Opx coronas are present which suggest PT conditions near the invariant points [Sill] and [Opx] (Fig. 8), i.e. at a lower P than the invariant point [Cd]. However, samples from Paderu displaying reaction coronas inferred to have formed near the invariant points [Cd], [Sp], [Opx], and [Sill] are found in localities only a few hundred meters apart. Such an abrupt changes of P over such a small area seems unlikely. The experimental data of Newton (1972) demonstrate that hydrous cordierite is stable at higher pressures (up to 3–4 kb) than anhydrous cordierite. It is, therefore, necessary to evaluate the effects of the additional component Fe_2O_3 and the activity of water on the mineral parageneses.

The diagrams μ_{FeO} vs. $\mu_{Fe_2O_3}$ and μ_{H_2O} vs. $\mu_{Fe_2O_3}$ portray qualitatively the possible factors responsible for the difference in behavior of natural sapphirine and spinel-bearing parageneses from the MAS and FMAS model systems. The stoichiometric coefficients of the reactions in the MAS and FMAS systems have been calculated from the mineral compositions given in Table 7, which are based on the microprobe data listed in Tables 3–6. These reactions have been used to construct the petrogenetic grids $\mu_{Fe_2O_3}$ vs. μ_{FeO} and μ_{H_2O} vs. $\mu_{Fe_2O_3}$ at a constant pressure and temperature (900 °C/6·5 kb). The relative slopes of the reactions for these grids have been calculated from the stoichiometric coefficients of the pertinent oxides, viz. FeO, Fe_2O_3, and H_2O, following the procedure given in Ferry & Burt (1982).

TABLE 7

Mineral compositions used for calculating the stoichiometric coefficients of the reactions in the MAS, MASH, and FMASH systems

	Composition					
Minerals	*MgO*	*FeO*	Fe_2O_3	Al_2O_3	SiO_2	H_2O
Spinel						
MAS	1	—	—	1	—	—
FMAS	0·55	0·45	0·042	0·958	—	—
Sapphirine						
MAS	7	—	—	9	3	—
FMAS	5·75	1·25	0·33	8·67	3	—
Cordierite						
MAS	2	—	—	2	5	—
MASH	2	—	—	2	5	0·5*
FMAS	1·8	0·2	—	2	5	—
FMASH	1·8	0·2	—	2	5	0·5*
Orthopyroxene						
MAS	0·9	—	—	0·1	0·9	—
FMAS	0·625	0·275	0·012	0·088	0·9	—
Garnet						
MAS	3	—	—	1	3	—
FMAS	1·5	1·5	—	1	3	—
Sillimanite						
MAS	—	—	—	1	1	—
FMAS	—	—	0·014	0·986	1	—
Quartz	—	—	—	—	1	—

* H_2O-content of cordierite from Newton & Wood (1979) at 900 °C/6·5 kb.

In FMAS and FMASH system, 'F' includes Fe^{2+} and Fe^{3+} in the table. Fe^{3+}-bearing minerals would represent the system Fe–Mg–Al–Si–O–H.

$\mu_{Fe_2O_3}$ *vs.* μ_{FeO} *diagram*

The effect of the relative difference in the Fe^{2+}/Mg and Fe^{3+}/Fe^{2+} ratios in the minerals involved in the reactions of the Fe–Mg–Al–Si–O system can be portrayed in the diagram $\mu_{Fe_2O_3}$ vs. μ_{FeO}, assuming a constant pressure and temperature (Fig. 9). Because μ_{FeO} and $\mu_{Fe_2O_3}$ affect the FeO/MgO and Fe_2O_3/FeO ratios in the rocks, it is possible to relate the host rock FeO and Fe_2O_3 contents with the phase relations projected onto the MAS system. This approach is an alternative to the *P–X* (Fe–Mg) and *T–X* (Fe–Mg) sections through the *P–T–X* (Fe–Mg) space used by Thompson (1976) to show the compositional variation in the coexisting phases that are participating in continuous reactions.

The $\mu_{Fe_2O_3}$ vs. μ_{FeO} diagram (Fig. 9) suggests:

(1) Sapphirine should be unstable at high μ_{FeO}, in agreement with the restricted occurrence of sapphirine in rocks of high X_{Mg} bulk compositions (Seifert, 1974). The formation of the Sa + Qz and Sp + Qz associations should be favoured by conditions of high oxygen fugacity (i.e. high $\mu_{Fe_2O_3}$). The prevalence of high oxygen fugacity during the Early Stage of reaction-corona formation in the Sa–Sp–Qz rocks of Paderu is evident from: (1) high contents of Fe^{3+} in spinel, sapphirine and sillimanite; (2) higher Fe^{3+} in sapphirine from the Sa + Qz association than in average sapphirine in the analysed rocks of the Paderu area; and (3) the ubiquitous association of ilmeno-hematite/hemo-ilmenite associated with spinel in the different types of coronas.

(2) At relatively high oxygen fugacities, as μ_{FeO} increases, the assemblages Sa + Qz (rock type A-1-1), Sa + Sp + Qz (A-2) and Sp + Qz (rock type B) should appear in succession. Thus it is evident that at similar *PT* conditions there is considerable overlap in the stability fields of Sp–Qz and Sa–Qz, due to variations in the activities of Fe and O_2. Note that in the Paderu

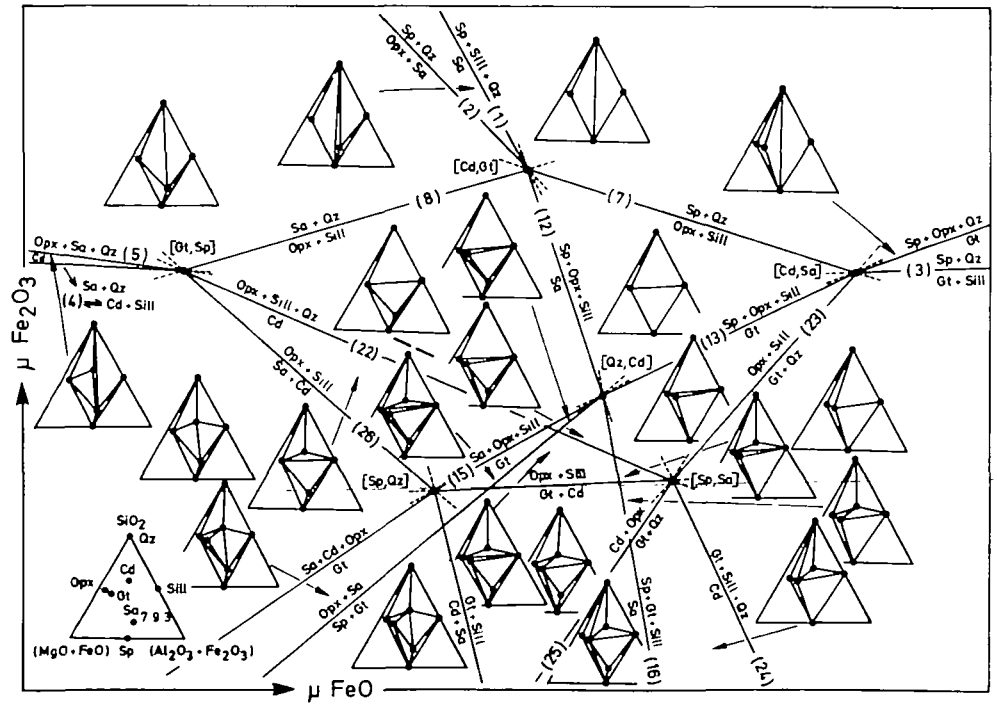

FIG. 9. $\mu_{Fe_2O_3}$ vs. μ_{FeO} diagram at constant *PT* (900 °C/6·5 kb, mean estimates of the thermal peak of metamorphism in the area).

area both spinel and sapphirine begin to react with quartz simultaneously to form reaction coronas (see Fig. 2A). On the other hand, Fig. 8 shows that the Sp–Qz association is stable at higher temperature than the Sa + Qz assemblage.

(3) The invariant points [Cd, Sa] and [Cd, Gt] are stable in the $\mu_{Fe_2O_3}$ vs. μ_{FeO} diagram (Fig. 9) at high $\mu_{Fe_2O_3}$, as is evident from the coronas and the related reactions. The invariant points [Cd, Sa] and [Cd, Gt] correspond to the univariant reactions (9) and (6) respectively, emerging from the invariant points [Cd] in the *PT* grid shown in Fig. 8. This suggests that the invariant point [Cd] in the *PT* grid could be stable at high oxygen fugacity (cf. Hensen, 1986) and may be metastable in the synthetic FMASH system under reducing conditions (Hensen, 1971; Hensen & Green, 1971).

(4) The $\mu_{Fe_2O_3}$ vs. μ_{FeO} diagram suggests that crystallization of garnet should be favoured in a reducing environment, in agreement with the experimental data of Hsu (1968) and in rocks of FeO-richer bulk compositions (high μ_{FeO}).

(5) The rock types A-2-1 and B-1-1 display corona textures suggesting formation through the reactions near the invariant point [Cd, Gt]. On the other hand, the rock types A-2-2, A-2-3, and B-1-2 are characterized by reaction coronas and other reaction textures evidently related to the reactions involved near the invariant points [Cd, Gt], [Qz, Cd], and [Sp, Sa]. A decrease in oxygen fugacity during the crystallization of these rocks, i.e. reaction coronas formed due to reactions at the invariant points [Cd, Gt] to [Sp, Sa], may be at least partly attributed to earlier crystallization of the minerals with a higher content of Fe^{3+}, such as sapphirine, spinel and ilmeno-hematite/hemo-ilmenite. These minerals no longer react with minerals in the matrix, because of armoring by coronas formed through the reactions at the invariant point [Cd, Gt]. Thus the 'effective' Fe_2O_3-content of the matrix was reduced, resulting in the formation of later coronas and other reaction textures near the [Qz, Cd] and [Sp, Sa] under less oxidizing conditions. Thus sapphirine and spinel in the Sp–Sa–Sill–Gt corona (reaction 16) have lower Fe^{3+} compared to those associated with the Sp–Sa–Sill–Opx corona (reaction 12).

(6) The type C-1 rocks lacking spinel and sapphirine do not display reaction coronas, but the textural and chemographic relations suggest reactions near the invariant point [Sp, Sa]. Low contents of Fe_2O_3 in sillimanite, the common presence of ilmenite, and the absence of ilmeno-hematite/hemo-ilmenite attest to crystallization under conditions of relatively low oxygen fugacity (low $\mu_{Fe_2O_3}$) compared to the type A and B assemblages.

(7) Rock type A-1-1 has coronas and other reaction textures suggesting formation near the invariant points [Gt, Sp] and [Sp, Sa]. Sapphirine, cordierite, and orthopyroxene, in the corona formed through the reactions at the invariant point [Gt, Sp], contain higher X_{Mg} in the A-1-1 rocks than in the corresponding A-2 and B assemblages.

(8) Rock type B-2-1 is characterized by reaction coronas which suggest their crystallization in Fe_2O_3- and FeO-rich bulk compositions (high $\mu_{Fe_2O_3}$ and μ_{FeO}) near the invariant point [Cd, Sa]. This is evident from lower X_{Mg} in garnet, spinel, and orthopyroxene than in rock type A, and from the high content of Fe_2O_3 in sillimanite.

The μ_{H_2O} vs. $\mu_{Fe_2O_3}$ diagram at constant PT

Variable water activity is portrayed in such a diagram in Fig. 10. The invariant points not involving cordierite reactions are metastable in this grid, because the slopes of the reactions are parallel to the μ_{H_2O}-axis. The grid suggests that crystallization of cordierite should be favoured by an increase in the activity of water (μ_{H_2O}), as demonstrated experimentally by Newton (1972). The corona type Sp–Cd occurs in rock type B-1-2. It is evident from the grid that this corona can form at high $\mu_{Fe_2O_3}$ and high μ_{H_2O} through the reaction (17). Similarly, the

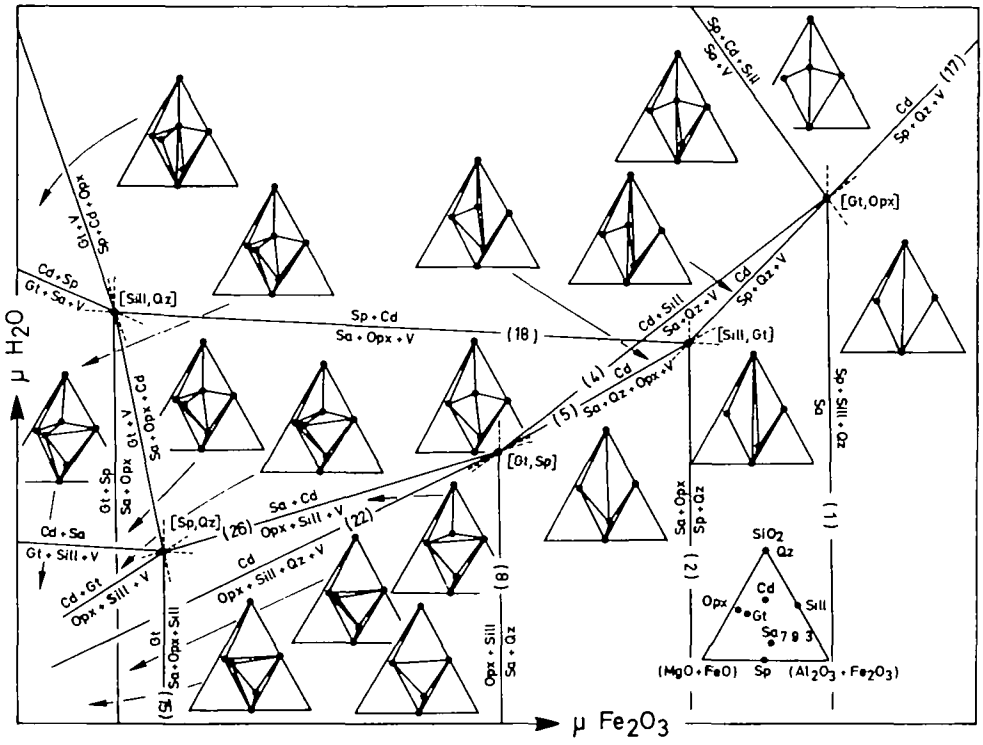

FIG. 10. μ_{H_2O} vs. $\mu_{Fe_2O_3}$ diagram at constant *PT* (see Fig. 9).

corona type Sp–Sa–Cd–Opx (reaction 18) in rock type A-2-3 may form at high μ_{H_2O} and moderate to high $\mu_{Fe_2O_3}$. An increase in μ_{H_2O} is indicated by the low analytical totals of the cordierites.

Comparison of the P–T–X *relationships with other areas of Sa–Sp–Qz rocks*

The relative FeO and Fe_2O_3 contents in the bulk compositions of the sapphirine–spinel–quartz-bearing rocks from other terranes can be deduced from the types of coronas and other reaction textures, if we assume that the *PT* conditions during the crystallization of these rocks were similar to those portrayed in the $\mu_{Fe_2O_3}$ vs. μ_{FeO} diagram (Fig. 9).

At Peekskill, New York (Caporuscio & Morse, 1978) and Wilson Lake, Labrador (Morse & Tally, 1971; Meng & Moore, 1972), the sapphirine–spinel–quartz rocks display reaction coronas, viz. Sp–Sill–Opx, Sp–Sa–Opx and Sa–Sill–Opx (reaction 7, 2, and 8), suggesting their crystallization near the invariant point [Cd, Gt]. The prevalence of high oxygen fugacity during their crystallization is evident from high Fe^{3+}-contents of sapphirine, spinel, and sillimanite and the ubiquitous presence of ilmeno-hematite/hemo-ilmenite.

The sapphirine–quartz rocks described by Grew (1980*a*) from Enderby Land, Antarctica, are Mg-rich and contain low Fe^{3+} in sapphirine and sillimanite. The textural relations in these rocks document evidence for reactions (4), (5), and (8), which suggests relative μ_{FeO}–$\mu_{Fe_2O_3}$ conditions near those of invariant point [Gt, Sp]. Ellis *et al.* (1980) studied sapphirine-quartz rocks from other localities in Enderby Land. The corona textures reported by them, viz. Sa–Cd–Sill (reaction 4), Sa–Sill–Cd–Opx (reaction 26), Sp–Sa–Sill–Gt (reaction

16) and Sa–Sill–Cd–Gt (reaction Gt + Sill = Sa + Cd), suggest relative $\mu_{Fe_2O_3}$–μ_{FeO} conditions near the invariant points [Gt, Sp] and [Sp, Qz]. The lower Fe^{3+}-contents of sapphirine, spinel and sillimanite, and higher X_{Mg} of the Fe/Mg minerals, when compared with these same minerals of rock type A-2 from this study, are consistent with the relative activities of Fe_2O_3 and FeO portrayed in Fig. 9.

The estimated mean *PT* conditions of the thermal peak of metamorphism of the Paderu rocks, 900 ± 60 °C/$6{\cdot}5 \pm 0{\cdot}7$ kb, may be compared with the *PT* conditions inferred from other terranes characterized by Sa + Qz parageneses e.g., Enderby Land, Antarctica: 900 °C/7 $\pm$ 1 kb (Grew, 1980*a*), 930–980 °C/8–10 kb (Ellis, 1980; Ellis *et al.*, 1980) and 900–950 °C, with pressures increasing from 6–8 kb in the Tula Mountains to 9–11 kb in Amundsen Bay (Harley, 1985); Labwor, Uganda: 800–900 °C/~6·5 kb (Nixon *et al.*, 1984); Gruf complex, Italian Central Alps: 830 ± 70 °C/10 ± 2 kb (prismatic sapphirine stage) and 750 ± 100 °C/5 $\pm$ 1 kb (cordierite and symplectite stage) (Droop & Bucher-Nurminen, 1984) and Limpopo belt, southern Africa: >800 °C/>7–8 kb (Schreyer *et al.*, 1984).

The Sa–Sp–Qz rocks of the Paderu area have a special significance, regarding the early crustal evolution in southern India. The granulite facies rocks south and south-west of Paderu, i.e. in southern Karnataka and Tamil Nadu, are inferred to have formed at the thermal peak near 800 °C and pressures ranging from 6 to 10 kb (Harris *et al.*, 1982; Jarnardhan *et al.*, 1982; Newton & Perkins, 1982; Grew, 1982; Raith *et al.*, 1982, 1983; Sen & Bhattacharya, 1984 and others). *PT* conditions (thermal peak) of 750 ± 40 °C/$7 \pm 0{\cdot}4$ kb and 800 ± 50 °C/$6{\cdot}8 \pm 0{\cdot}7$ kb have been estimated for the silica-deficient sapphirine–gedrite–sillimanite–cordierite–spinel rocks of Kiranur, Tiruchchirapalli, (Lal *et al.*, 1984) and sapphirine–cordierite–orthopyroxene–spinel–garnet granulites of Ganguvarpatti, Madurai (Mohan *et al.*, 1986), respectively.

The Sa–Sp–Qz rocks of Paderu, on the other hand, formed within the above mentioned pressure range (6–10 kb) but at higher temperatures (~900 °C). It is thus likely that these rocks represent a 'hot spot' region within the granulite facies terrane of southern India. Mantle diapirs or high-temperature mantle-derived liquids coalescing at the base of the crust could produce a marked inflection in a steady-state geotherm. An apparently exceptional geothermal gradient could then prevail in the overlying crust (Ellis, 1980).

P–T–t RELATIONSHIPS

The estimated *PT* conditions and total crustal thickness in Paderu can be used to place constraints on the thermal state of the Precambrian continental crust. The mean pressure of $6{\cdot}5 \pm 0{\cdot}7$ kb implies an overburden of 23 ± 2 km. If we assume an average crustal thickness for the Precambrian terrane of southern India of 35 km at the present time (Kaila *et al.*, 1979), crustal thickness at the time of metamorphism may have been ~60 km. The pressure difference of 1·5 kb inferred from garnet core and rim compositions suggests uplift of about 5 km. Unfortunately no geochronological data are available for calculating the rate of uplift.

England & Richardson (1977), Thompson & England (1984), and Schreyer (1985), amongst others, proposed a 'clockwise' loop for the *P–T–t* path with a steep, near isothermal retrograde trajectory. Such a *P–T–t* path may be characteristic of metamorphic belts formed by continental collision or overthrust processes, where rapid erosion rates of the tectonically thickened pile predominates. By contrast, in other metamorphic belts moderate to isobaric cooling paths are evident, presumably due to crustal thickening by magma-accretion when conductive relaxation dominates over erosion. In the granulite facies terrane of Antarctica, Ellis (1980) suggested the magma-accretion model, which is characterized by near isobaric cooling, while Harley (1985) proposed a combination of the magma-accretion model and

tectonic thickening by continental collision. For the rocks of Paderu, we may consider two plausible models for the retrograde *P–T–t* path:

(1) The mean *PT* estimates for the core and rim compositions suggest a mildly decompressive retrograde *P–T–t* path, which can be explained by the combined model proposed by Harley (1985) for the granulite facies rocks of Antarctica.

(2) On the other hand, pressure estimates through the Gt–Opx–Plag–Qz (Newton & Perkins, 1982) and Al-content of Opx coexisting with Gt (Harley & Green, 1982), disregarding the other models, range from >9–4 kb at the mean temperatures of 900 ± 60 °C (core) and 760 ± 50 °C (rim), respectively. This suggests an uplift of ~16 km and a total crustal thickness of ~67 km. These *PT* estimates, which we assume to represent 'frozen-in' points on the geotherm curve, imply a moderate to steep decompressive retrograde *P–T–t* path and rapid uplift while the temperature was near the thermal peak of metamorphism (Fig. 11). A similar, nearly isothermal decompressive retrograde *P–T–t* trajectory has been

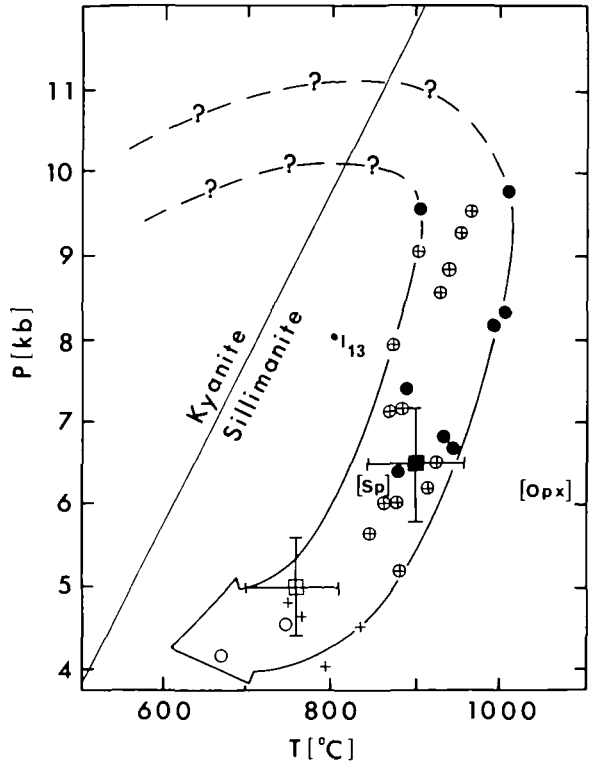

FIG. 11. *P–T–t* diagram showing moderate to steep decompressive retrograde trajectory based on the *PT* estimates from geothermobarometry. Crossed circles and crosses—estimates of *PT* for the garnet core and rim compositions, respectively, calculated graphically by simultaneous solutions of the Fe–Mg exchange reaction between Gt–Opx (Harley, 1984) and the Al-contents of Opx coexisting with Gt (Harley & Green, 1982) for *P* and *T*. The intersection of the two curves for these equations yields *P* and *T* for the given Gt–Opx pair. Large dots and circles—estimates of *PT* for the core and rim compositions, respectively, calculated graphically as above, through the Gt–Opx Fe–Mg exchange reaction (Harley, 1984) and Gt–Opx–Plag–Qz equilibrium (Newton & Perkins, 1982). Mean *PT* estimates from the different models of geothermobarometry (see text) for the core (filled square) and rim (open square), with vertical and horizontal bars indicating the standard deviation, are also shown. I_{13}—invariant point for the MAS system (Newton, 1972, with $Sa_{2:2:1}$), invariant point [Sp]and [Opx]—calculated by Grew (1982) for the FMAS system ($Sa_{7:9:3}$), and kyanite ⇌ sillimanite equilibrium (Holdaway, 1971). The univariant reactions emerging from the invariant points I_{13}, [Sp] and [Opx] have been omitted for clarity, these are given in Fig. 8.

proposed for the sapphirine-bearing rocks of the Gruf complex, Italian Central Alps (Droop & Bucher-Nurminen, 1984) and Limpopo belt (Windley *et al.*, 1984), in agreement with the model of crustal thickening by continental collision and overthrusting.

The preservation of spectacular multi-phase reaction coronas in the Sa–Sp–Qz rocks of Paderu can thus be attributed to: (a) a moderate to steep decompressive retrograde *P–T–t* path, suggesting rapid uplift at high temperatures near the thermal peak of metamorphism; (b) refractory or less reactive minerals, e.g. Sa, Sp, Sill, Gt etc., participating in the reactions forming coronas; and (c) rather anhydrous conditions of metamorphism, because hydration reaction (26–30, see above) of the Late Stage are likely to obliterate the coronas (rock types C, in contrast to types A and B, are devoid of reaction coronas. Instead, evidence of Late Stage reactions, during which retrograde biotite formed, is widespread in type C).

The investigation of sapphirine-bearing rocks, which preserve signatures of the different stages of metamorphic crystallization in the form of coronas, symplectites and other reaction textures, can be highly rewarding in unraveling the complex Precambrian crustal evolution.

ACKNOWLEDGEMENTS

H. Upadhayay expresses his gratitude to the Council of Scientific and Industrial Research, Government of India, for financial assistance as a junior research fellow. R. K. Lal is thankful to the Alexander von Humboldt-Stiftung, Bonn for the award (renewal) of a fellowship, during which this study has in part been carried out. The authors are thankful to F. Seifert, J. C. Schumacher, M. Raith, G. T. R. Droop, and E. S. Grew for their comments and suggestions on the manuscript. We are grateful to Mrs. Lund for her assistance in microprobe analysis, drafting the figures and typing the manuscript, and to A. Richter for taking the photo-micrographs. The final version of the paper has been completed during the tenure of financial support from the Stiftung Volkswagenwerk, which is thankfully acknowledged.

REFERENCES

Ackermand, D., & Lal, R. K., 1985. Koronagefüge in Sapphirin–Spinell–Quartz—führenden Gesteinen von Paderu, Andhra Pradesh, Indien. *Fortschr. Miner.* **63**, 4.

Aswathanarayan, U., 1964. Isotopic ages from the Eastern Ghats and Cuddapahs of India. *Geophys. Res.* **69**, 3479–86.

Berg, J. H., & Wheeler, E. P. II, 1976. Osumilite of deep-seated origin in the contact aureole of the anorthositic Nain Complex, Labrador. *Am. Miner.* **61**, 29–37.

Bohlen, S. R., & Essene, E. J., 1977. Feldspar and oxide thermometry in the Adirondack Highlands. *Contr. Miner. Petrol.* **62**, 153–69.

—— Wall, V. J., & Boettcher, A. L., 1983*a*. Experimental investigation and application of garnet granulite equilibria. *Ibid.* **83**, 52–61.

—— —— —— 1983*b*. Experimental investigations and geological application of equilibria in the system $FeO–TiO_2–Al_2O_3–SiO_2–H_2O$. *Am. Miner.* **68**, 1049–58.

Bourne, J. H., 1978. Metamorphism in the eastern and south-western portions of the Grenville Province. In: Fraser, J. A., & Heywood, N. W., (Eds) *Metamorphism in the Canadian Shield*. Geol. Surv. Canada Pap. 78-10, 315–28.

Buhl, D., Grauert, B., & Raith, M., 1983. U–Pb zircon dating of Archean rocks from the South India Craton: results from amphibolite to granulite facies transitions zone at Kabbal quarry, southern Karnataka. *Fortschr. Miner.* **61**, 43–45.

Caporuscio, F. A., & Morse, S. A., 1978. Occurrence of sapphirine plus quartz at Peekskill, New York. *Am. J. Sci.* **278**, 1334–42.

Chatterjee, N. D., & Schreyer, W., 1972. The reaction enstatite$_{ss}$ + sillimanite = sapphirine$_{ss}$ + quartz in the system $MgO–Al_2O_3–SiO_2$. *Contr. Miner. Petrol.* **36**, 49–62.

Crawford, A. R., 1969. India, Ceylon, Pakistan, New age data and comparisons. *Nature*, **223**, 380–4.

Crookshank, H., 1930. Note on sapphirine in the Vizagapatnam district. *Geol. Surv. India Rec.* **63**, 446–8.

Dallwitz, W. B., 1968. Coexisting sapphirine and quartz in granulite from Enderby Land, Antarctica. *Nature*, **219**, 476–77.

Droop, G. T. R., & Bucher-Nurminen, K., 1984. Reaction textures and metamorphic evolution of sapphirine-bearing granulites from the Gruf Complex, Italian Central Alps. *J. Petrology*, **25**, 766–803.

Ellis, D. J., 1980. Osumilite–sapphirine–quartz granulites from Enderby Land, Antarctica: *PT* conditions of metamorphism, implication for garnet–cordierite equilibria and the evolution of the deep crust. *Contr. Miner. Petrol.* **74**, 201–10.

—— Green, D. H., 1979. An experimental study of the effect of Ca upon garnet–clinopyroxene Fe–Mg exchange equilibria. *Ibid.* **71**, 13–22.

—— Sheraton, J. M., England, R. N., & Dallwitz, W. B., 1980. Osumilite–sapphirine–quartz granulites from Enderby Land, Antarctica—mineral assemblages and reactions. *Ibid.* **72**, 123–43.

England, P. C., & Richardson, S. W., 1977. The influence of erosion upon the mineral facies of rocks from different metamorphic environments. *J. geol. Soc. Lond.* **134**, 201–13.

Ferry, J. M., & Burt, D. M., 1982. Characterization of metamorphic fluid composition through mineral equilibria. In, *Characterization of Metamorphism Through Mineral Equilibria*. Reviews in Mineralogy, Vol. 10, Mineral. Soc. Am., Ferry, J. M. (Ed.) Chapter 6, 207–262.

Grasty, R. L., & Leelanandam, C., 1965. Isotopic ages of basic charnockite and khondalite from Kondapalli, Andhra Pradesh. *Miner. Mag.* **35**, 529–35.

Grew, E. S., 1980*a*. Sapphirine + quartz association from Archean rocks of Enderby Land, Antarctica. *Am. Miner.* **65**, 821–36.

—— 1980*b*. Sillimanite and ilmenite from high-grade metamorphic rocks of Antarctica and other areas. *J. Petrology*, **21**, 39–68.

—— 1982. Sapphirine, kornerupine and sillimanite + orthopyroxene in the charnockitic region of South India. *J. Geol. Soc. India*, **23**, 469–505.

—— 1983. A grandidierite–sapphirine association from India. *Miner. Mag.* **47**, 401–3.

Hamm, H. W., & Vieten, K., 1971. Zur Berechnung der kristall-chemischen Formel und des Fe^{3+}-Gehaltes von Klinopyroxenen aus Elektronenstrahl-Mikroanalysen. *N. Jb. Miner. Mh.* 310–14.

Harley, S. L., 1984. An experimental study of the partitioning of Fe and Mg between garnet and orthopyroxenes. *Contr. Miner. Petrol.* **86**, 359–73.

—— 1985. Garnet-orthopyroxene bearing Granulites from Enderby Land, Antarctica: Metamorphic pressure–temperature–time evolution of Archean Napier Complex. *J. Petrology*, **26**, 819–56.

—— Green, D. H., 1982. Garnet–orthopyroxene barometry for granulites and peridotites. *Nature*, **300**, 697–701.

Harris, N. B. W., Holt, R. W., & Drury, S. A., 1982. Geobarometry, geothermometry and Late Archean geotherms from the granulite facies terrane of south India. *J. Geol.* **90**, 509–27.

Hensen, B. J., 1971. Theoretical phase relations involving cordierite and garnet in the system $MgO–FeO–Al_2O_3–SiO_2$. *Contr. Miner. Petrol.* **33**, 191–214.

—— 1986. Theoretical phase relations involving cordierite and garnet revisited: the influence of oxygen fugacity on the stability of sapphirine and spinel in the system Mg–Fe–Al–Si–O. *Contr. Miner. Petrol.* **92**, 362–7.

—— Green, D. H., 1971. Experimental study of the stability of cordierite and garnet in pelitic compositions at high pressure and temperatures. I. Compositions with excess alumino-silicate. *Ibid.* **33**, 309–30.

Higgins, J. B., Ribbe, P. H., & Herd, R. K., 1979. Sapphirine I: Crystal chemical contributions. *Ibid.* **68**, 349–56.

Holdaway, M. J., 1971. Stability of andalusite and the aluminium silicate phase diagram. *Am. J. Sci.* **271**, 97–131.

Holmes, A., 1955. Dating the Precambrian of Peninsular India and Ceylon. *Proc. geol. Ass. Canada*, **7**, 81–106.

Hsu, L. C., 1968. Selected phase relations in the system Al–Mn–Fe–Si–O–H: A model for garnet equilibria. *J. Petrology*, **9**, 40–83.

Janardhan, A. S., Newton, R. C., & Hansen, E. C., 1982. The transformation of amphibolite facies gneiss to charnockite in southern Karnataka and northern Tamil Nadu, India. *Contr. Miner. Petrol.* **79**, 130–49

Kaila, K. L., Roy Chowdhury, K., Reddy, P. R., Krishna, V. G., Narain, H., Subbotin, S. I., Sollugub, V. B., Chekunov, A. V., Kharetchko, G. E., Lazarenko, M. A., & Ilehenko, T. V., 1979. Crustal structure along Kavali-Udipi profile in the Indian peninsular shield from deep seismic sounding. *J. geol. Soc. India*, **20**, 307–33.

Karsakov, L. P., Shuldiner, V. I., & Lennikov, A. M., 1975. Granulite Complex of the eastern part of the Fold Province and the Chogar facies of depth. *Isvestiya Akad. Nauk. SSSR, Ser. Geol.* **5**, 47–61 (in Russian).

Lal, R. K., Ackermand, D., Raith, M., Raase, P., & Seifert, F., 1984. Sapphirine-bearing assemblages from Kiranur, Southern India: A study of chemographic relationships in the $Na_2O–FeO–MgO–Al_2O_3–SiO_2–H_2O$ system, *N. Jb. Miner. Abh.* **150**, 121–52.

Meng, L. K., & Moore, J. M. (Jr), 1972. Sapphirine-bearing rocks from Wilson Lake, Labrador. *Can. Miner.* **11**, 777–90.

Middlemiss, C. S., 1904. Note on a sapphirine-bearing rock from Vizagapatnam district. *Geol. Surv. India Rec.* **31**, 38–42.

Mohan, A., Ackermand, D., & Lal, R. K., 1986. Reaction textures and *P–T–X* trajectory in the sapphirine–spinel–bearing granulites from Ganguvarpatti, southern India. *N. Jb. Miner. Abh.* **154**, 1–19.

Moore, P. B., 1969. The crystal structure of sapphirine. *Am. Miner.* **54**, 31–49.

Morse, S. A., & Talley, J. H., 1971. Sapphirine reactions in deep seated granulites near Wilson Lake. Central Labrador, Canada. *Earth planet. Sci. Lett.* **10**, 325–28.

Narayanaswami, S., 1964. Tectonic problems of the Precambrian rocks of Peninsular India: Symposium on Tectonics. Nat. Inst. Sci. India and Indian Geophy. Union, Special Number, 86.

Newton, R. C., 1972. An experimental determination of the high-pressure stability limits of magnesian cordierite under wet and dry conditions. *J. Geol.* **80,** 398–420.

—— Perkins III, D., 1982. Thermodynamic calibration of geobarometers based on the assemblages garnet–plagioclase–orthopyroxene (clinopyroxene)–quartz. *Am. Miner.*, **67,** 203–22.

—— Wood, B. J., 1979. Thermodynamics of water in cordierite and some petrologic consequences of cordierites as hydrous phase. *Contr. Miner. Petrol.* **68,** 391–405.

Nixon, P. H., Grew, E. S., & Condiffe, E., 1984. Kornerupine in a sapphirine–spinel granulite from Labwar Hills, Uganda. *Miner. Mag.* **48,** 550–2.

—— Reedman, A. J., & Burns, L. K., 1973. Sapphirine-bearing granulites from Labwar, Uganda. *Ibid.* **39,** 420–28.

Perraju, P., Kovāch, A., & Svingor, E., 1979. Rubidium-strontium ages of some rocks from parts of the Eastern Ghats in Orissa and Andhra Pradesh, India. *J. geol. Soc. India*, **20,** 290–6.

Raith, M., Raase, P., Ackermand, D., & Lal, R. K., 1982. The Archean Craton of Southern India: Metamorphic evolution and *P–T* conditions. *Geol. Rundsch.* **71,** 280–90.

—— —— —— —— 1983. Regional geothermobarometry in the granulite facies terrane of South India *Trans R. Soc. Edinburgh: Earth Sci.* **73,** (for 1982), 221–4.

Ramakrishnan, M., Moorbath, S., Taylor, P. N., Anantha Iyer, G. V., & Vishwanatha, M. N., 1984. Rb–Sr and Pb–Pb whole rock isochron ages of basement gneisses in Karnataka craton. *J. geol. Soc. India*, **25,** 20–34.

Rao, L. H., 1980 Mineralogy and petrology of sapphirine-bearing and associated rocks of Paderu area, Vishakhapatnam district, Andhra Pradesh, India Unpublished Ph.D. thesis Andhra University, Waltair, India.

Robinson, P., & Jaffe, H. W., 1969. Aluminous enclaves in gedrite–cordierite gneiss from southwestern New Hampshire. *Am. J. Sci.* **267,** 389–421.

Sarkar, A. Bhanumathi, L., & Balasubrahmanyan, M. N., 1981. Petrology, geochemistry and geochronology of the Chilka Lake igneous complex, Orissa state, India *Lithos*, **14,** 93–111.

Schreyer, W., 1985. Metamorphism of crustal rocks at mantle depths· High-pressure minerals and mineral assemblages in metapelites. *Fortschr. Miner.* **63,** 227–61.

—— Horrocks, P. C., & Abraham, K., 1984. High-magnesium staurolite in a sapphirine-garnet rock from the Limpopo belt, southern Africa. *Contr. Miner. Petrol.* **86,** 200–7.

—— Seifert, F., 1967. Metastability of an osumilite endmember in the system K_2O–MgO–Al_2O_3–SiO_2–H_2O and its possible bearing on the rarity of natural osumilites, *Ibid.* **14,** 343–58.

—— —— 1969. Compatibility relations of the aluminium silicates in the system MgO–Al_2O_3–SiO_2–H_2O and K_2O–MgO–Al_2O_3–SiO_2–H_2O at high pressures. *Am. J. Sci.* **267,** 371–88.

Seifert, F., 1974. Stability of sapphirine: A study of the aluminous part of the system MgO–Al_2O_3–SiO_2–H_2O. *J. Geol.* **82,** 173–204.

Sen, S., & Bhattacharya, A., 1984. An orthopyroxene-garnet thermometer and its application to the Madras charnockites *Contr. Miner. Petrol.* **68,** 64–71.

Sriramdas, A., & Rao, A. T., 1979. Charnockites of Visakhapatnam, Andhra Pradesh. *J. geol. Soc. India.* **20,** 512–7.

Thompson, A. B., 1976. Mineral reactions in pelitic rocks: I. Prediction of *P–T–X* (Fe–Mg) phase relations. *Am. J. Sci.* **276,** 401–24.

—— England, P. C., 1984. Pressure-temperature-time paths of regional metamorphism II. Thier inference and interpretation using mineral assemblages in metamorphic rocks. *J. Petrology*, **25,** 929–55.

Vinogradov, A., Tugarinov, A., Zhykov, C., Stapnikova, N., Bibikova, E., & Khorre, K., 1964. Geochronology of Indian Precambrian. Inter. Geol. Congress, 22nd Session, Part 10, 553–67.

Walker, T. L., & Collins, W. H., 1907. Petrological study of some rocks from Vizagapatnam district. *Geol. Surv. India. Rec.* **31,** 38—42.

Windley, B. F., Ackermand, D., & Herd, R. K., 1984. Sapphirine/kornerupine-bearing rocks and crustal uplift history of the Limpopo belt, southern Africa. *Contr. Miner. Petrol.* **86,** 342–58.